American Journal of
Electronics & Communication

'Society for Makers, Artists, Researchers and Technologists (SMART)' is an American publishing house committed to publish high quality research articles which can bring value and momentum to current research in the domain of Electronics and Communication Technology and allied fields. As a part of this, it has started an international journal titled "American Journal of Electronics & Communication".

"American Journal of Electronics & Communication" (AJEC) is an open access, indexed, multidisciplinary peer reviewed journal that provides a platform for academicians and researchers all over the globe, to publish their research articles related to current trends and developments in Electronics and Communication Technology like microwave, semiconductor devices, VLSI, signal processing, communication, Internet of Things, Machine Learning, Artificial Intelligence etc. The main objective of AJEC is to cultivate innovative ideas among young minds and thus provide a proper guidance to the new frontiers and emerging trends in Electronics & Communication Engineering.

The American Journal of Electronics & Communication makes a maximum effort to publish submitted papers as quickly as possible. Primary reviews would be completed within two months. The authors are then requested to make necessary changes/improvements to their manuscripts within a span of two-three weeks. The whole review process fully respects standard Ethical Guidelines for Peer Reviewers.

Editor in Chief

Prof. Bob Gill

British Columbia Institute of Technology

Research Interest: Sustainability, Sustainable Development, Renewable Energy Technologies, Power Generation, Energy Engineering, Energy Conversion, Energy Efficiency in Building Distributed Generation, Energy Saving Electricity, Energy Management, Energy Modeling, Solar Energy, Solar Radiation, Energy Utilization, Life-Cycle Assessment, Sustainable Energy, Alternative Energy, Clean Energy, Green Energy, Energy Modelling.

Managing Editor

Dr. Satyajit Chakrabarti

Institute of Engineering & Management

Research Interest: Machine Learning, IoT, Big Data Analytics, Data Mining, Algorithms, Robotics, Sensors, Human Computer Interface, Networking & MANET, Wireless Communication.

Dr. Malay Gangopadhyay

Institute of Engineering & Management

Research Interest: Microwave Technology, Antenna, IoT, Robotics, Wireless Communication.

Contents

Design of Multiband Microstrip Antenna Using Two Parasitic Ring Resonators for WLAN/WiMAX and C/X/Ku-Band Applications

Ahmed Boutejdar[1]
Microwave Engineering Department,
German Research Foundation (DFG)
Bonn, Germany
boutejdar69@gmail.com

Bishoy I. Halim[2]
Communications and Electronics Department,
Alexandria University
Alexandria, Egypt
gendibishoy@yahoo.com

Abstract—In this paper, a new planar monopole antenna for multiband applications is proposed. The antenna structure operates at five operating frequencies at 2.88 GHz, 7.58 GHz, 9.88 GHz, 11.59 GHz and 13.78 GHz which covers different communication frequency ranges. The proposed antenna consists of a quasi-modified rectangular radiating patch with a partial ground plane and two parasitic elements (open-loop-ring resonators) to serve as coupling-bridges. A stepped cut at lower corners of the radiating patch and the partial ground plane are used, to achieve the multiband features. The proposed antenna is manufactured on the Rogers RO 3010 substrate and is simulated and optimized using High Frequency Simulation System (HFSS). The antenna topology possesses an area of 41.04 x 29.98 x 1.6 mm³. The measured results demonstrate that, the candidate antenna has impedance bandwidths for -10 dB return loss and operates from 2.68 – 3.03 GHz, 7.33 – 7.84 GHz, from 9.66 – 10.03 GHz, from 11.46 – 11.78 GHz and from 13.69 – 13.88 which meet the requirements of the wireless local area network (WLAN), worldwide interoperability for microwave access (WiMAX), C- (Uplink), X- (Uplink) band and Ku- (Uplink) band applications. Acceptable agreement is obtained between measurement and simulation results. Experimental results show that the antenna is successfully simulated and measured, and the tri-band antenna can be achieved by adjusting the lengths of the three elements and gives good gains across all the operation bands.

Keywords— Planar Monopole Antenna; HFSS; WLAN; WiMAX; C; X & Ku.

I. INTRODUCTION

With rapid development of wireless communication systems, one of the key issues is the design of compact multi-band antenna while providing wideband characteristic over the whole operating band, especially for wireless local area network (WLAN: 2.4-2.48, 5.15- 5.35, 5.725-5.85GHz) and worldwide interoperability for microwave access (WiMAX: 2.5-2.69, 3.4-3.69 GHz), where it plays a major importance. Consequently, a number of planar antennas using several topologies have been experimentally characterized. In addition, other methods to progress the impedance bandwidth which do not include adjustment of the geometry of the planar antenna have been examined [1-4]. It is a well- known fact; Commercial UWB systems demand compact and low-cost antennas with omnidirectional radiation patterns and large bandwidth [1].

Microstrip monopole antennas illustrate truly appealing physical characteristics features, such as uncomplicated structure, compactness and low-cost of fabrication process, low profile of antenna, light in weight, ease of installation process and integration with numerous feed types. Because of all these important features, planar monopole antennas are highly attractive to be employed in advanced UWB technologies, and recent research activity is being focused on them. Measure decreasing of the planar patch antenna has been carried out utilizing a few strategies such as the utilize of high dielectric constant substrates, adjustment of the conventional patch shapes, use of short circuits, shorting-pins technique [7]-[8]. Employing high dielectric constant substrates is a simple solution, but it shows narrow bandwidth, high loss and poor ability due to surface wave excitation [9]. In order to generate the single and multiple band-notched functions, respectively, single and multiple half- wavelength ring resonators [6] are incorporate in the radiation patch topology. In [7], band- notch function is reached by using a T-shaped coupled-parasitic element in the ground plane. Also, different planar inverted-F antennas (PIFA) designs have been proposed for several bands in newest researchers. Minimize dual band (PIFA) have been reported in [10, 11], and are reached using etched slotted radiated element. In [12-17], triple band small size composite-resonator monopole antenna designs for wireless communications were presented. Theses antennas are consisting of three resonant topologies. Two types of compact short-circuited resonators were used; stepped impedance and quarter-wave resonators. The narrowband services such WLAN, Wi-MAX and ITU may generate undesired interference with the UWB band. In order to avoid this problem, it is preferable to used antenna-topologies with noch-band features. However, there are some other existing narrowband services that may cause interference with the UWB band, such as WLAN, Wi-MAX and ITU. To solve this problem, it is desirable to design antennas with band-notched characteristic to reduce potential interference [2], [3]. To

avoid these interferences, there is Several researchers, who proposed multiple antenna design methods to produce the band-notched characteristic in the UWB band, such as photonic band-gap (PBG) structure, defected ground structure (DGS), defected microstrip structure (DMS) and using slotted the patch or ground through different slots [5].

In this work, a simple method for designing a quad-band small size monopole microstrip antenna with width band features has been presented. The proposed topology is simulated and optimized and manufactured on the 41.04 x 29.98 x 1.6 mm^3 Rogers duroid 6010 substrate of, permittivity 10.2. The simulation investigations are carried out using the Ansoft HFSS commercial software [12]. Details of the antenna design are described, and fabricated and simulated return loss, radiation pattern and antenna gain results are represented and discussed in the following section. The acceptable agreement between the experimental and the simulation results is observed. The Slight deviation between the simulated and fabricated results is due to the mismatching losses and the inexactitude of the manufacturing process. The parametric investigation is accomplished to understand the characteristics of the proposed antenna.

II. ANTENNA DESIGN

The topology of the proposed monopole microstrip multiband antenna, fed by 50 Ω microstrip feed line, is shown in Fig. 1. The design consists of modified structure of a conventional rectangular patch antenna and two loaded parasitic ring resonators around of the 50 Ω feed line. The radiating patch has a length L and a width W. The W and L are the width and length of the feed line, which connect the patch with SMA connector. On the other side of the substrate, a conducting partial ground plane is placed. The dimensions of the partial ground plane are width W_{gnd} and length L_{gnd} (see Fig. 1). The width of the microstrip feed line is fixed at 2 mm. The antenna is printed on a 41.04 x 29.98 x 1.6 mm^3 or about 0.924 λ_g x 0.910 λ_g x 0.048 λ_g with λ_g = 33 mm at 2.88 GHz (the first resonance frequency) and a Rogers duroid 3010 substrate of thickness 1.27 mm, permittivity 10.2, and loss tangent tanδ = 0.003. The design processes to reach the proposed antenna are depicted in Fig. 4. The investigated antenna is connected to a 50 Ω-SMA connector for signal transmission. The parameter values of the proposed design are illustrated in Fig. 1.
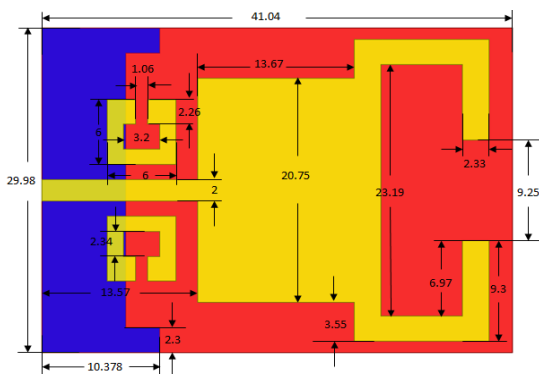
Fig. 1. Geometry of the proposed antenna structure.

III. RESULTS AND DISCUSSIONS

The investigate microstrip monopole DGS antenna with different design parameters, which can influence the bandwidth, were constructed, and the scattering results of the input impedance and radiation characteristics are demonstrated and discussed.

From Fig. 2 it is clear that, the proposed DGS antenna structure with partial ground has been achieved multiband operational frequencies. Fig. 4 illustrates the reflection coefficient characteristics of the proposed tri-band antenna. It can be seen that, in the proposed antenna, the three resonant modes are excited around the 2.88, 7.58 GHz, 9.88 GHz, 11.59 GHz and 13.78 GHz for WLAN/WiMAX and C/X/Ku-Band Applications for a $S_{11} \leq -10$dB.

In order to carry out different behaviors of this structure, several parameters of this antenna candidate are studied by varying one parameter, while others keep constant. Fig. 3 shows the steps process of the monopole antenna, the conventional square antenna (Fig. 3(a)), geometry without two ring resonators, (Fig. 3(b)), antenna with two ring resonators located along of the microstrip feed line.
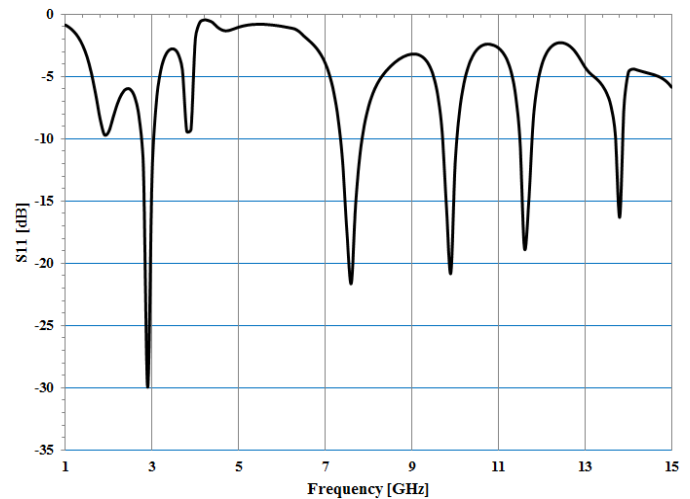
Fig. 2. The simulated S_{11} [dB] of the proposed DGS antenna.
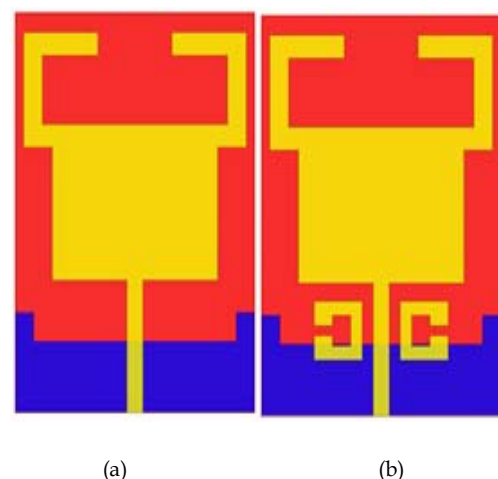
(a)   (b)
Fig. 3. Design evolution of the proposed antenna; (a) antenna I, (b) antenna II.

The achieved simulation results are computed using the high-frequency structure simulator (HFSS). Fig. 4 depicted the optimized multiband antenna.
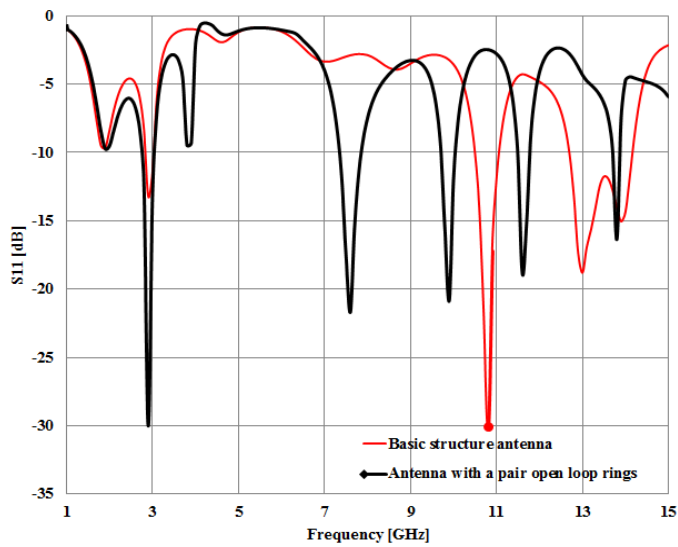
Fig. 4. Simulated reflection coefficient of various antenna designs.

As shown in Fig. 4, for the proposed antenna configuration, the conventional quasi square monopole can provide the fundamental and the next higher resonant radiation bands at 7.58 GHz, 9.88 GHz, 11.59 GHz and 13.78 GHz, respectively. As illustrated in Fig. 3, the ring resonators leads to an improvement in the broadband features and play a role in determining the sensitivity of impedance matching of such antenna. This is because it can influence the effects of electromagnetic coupling between the patch and the ground plane, hence the improvement its impedance bandwidth without any cost of size or expense. Depending on the above regenerated high frequencies at 7.58 GHz, 9.88 GHz, 11.59 GHz and 13.78 GHz can be observed.
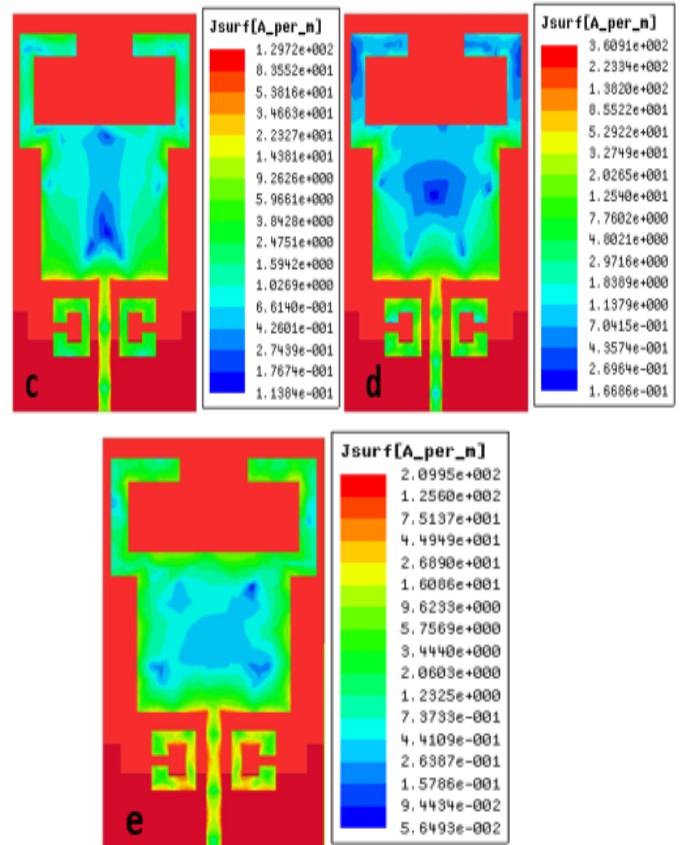
Fig. 5. Simulated surface current distribution of the proposed antenna at (a) 2.88GHz, (b) 7.58GHz, (c) 9.88GHz, (d) 11.59GHz and (e) 13.78GHz.

As shown in Fig.5, the current distributions of the proposed antenna structure at 2.88 GHz, 7.58 GHz, 9.88 GHz, 11.59 GHz and 13.78 GHz are presented respectively.

The simulated radiation patterns of the proposed microstrip antenna are presented in Fig. 6.
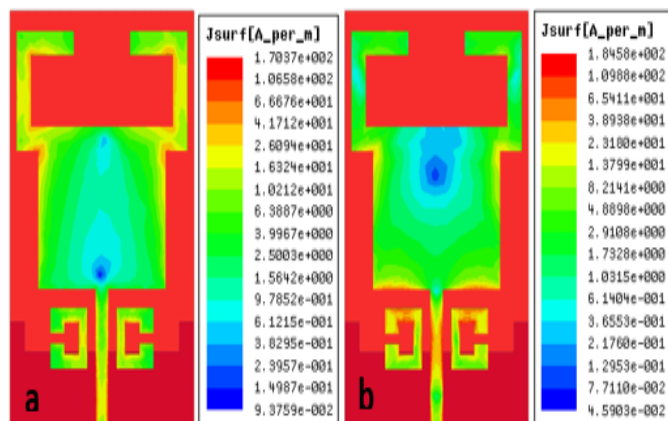
(a) Radiation pattern at 2.88 GHz   (b) Radiation pattern at 7.58 GHz

(c) Radiation pattern at 9.88 GHz

(d) Radiation pattern at 11.59 GHz

(e) Radiation pattern at 13.78 GHz

(f) Total Gain
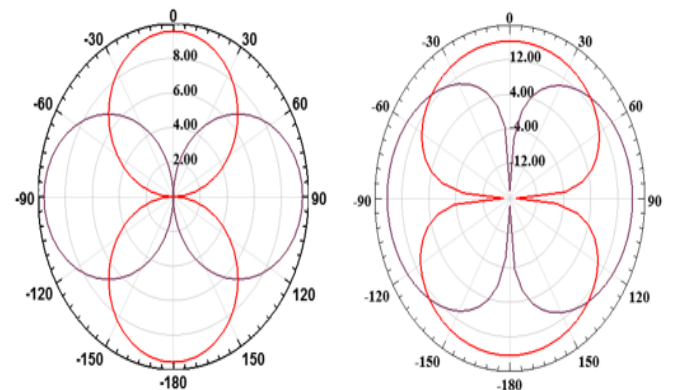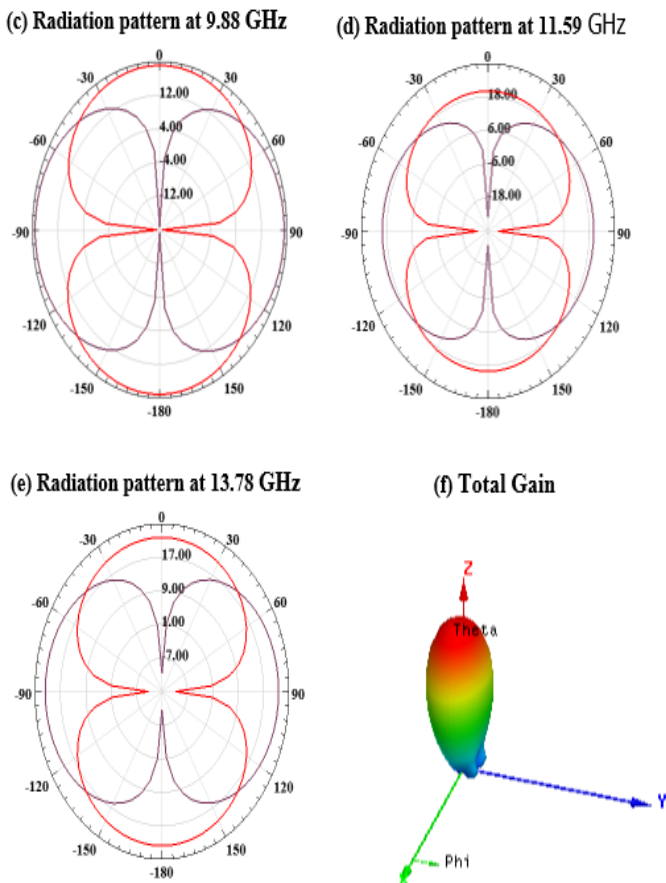
Fig.6. Simulated 2D radiation patterns of proposed antenna at respectively (a) 2.88 GHz, (b) 7.58 GHz, (c) 9.88 GHz, (d) 11.59 GHz, (e) 13.78 GHz and (f) 3D radiation pattern.

IV.   THE INVESTIGATION AND EXPERIMENTAL MEASUREMENTS

After the optimizing of the proposed triple-band antenna parameters, an experimental prototype of the final design was fabricated using printed circuit technology and tested. A photograph of the fabricated antenna is shown in Fig. 7. The measurements on the fabricated antenna were carried out using a vector network analyzer (VNA), over a relatively wide frequency range from 1- 15 GHz (Fig. 8).

Figure 9 illustrates the comparison between the simulated and measured reflection coefficient S11 of the proposed antenna. The measured results clearly indicate that the proposed antenna provides at least three resonance bands. From this figure, it is clear that the simulated and measured results show a reasonable agreement. The small discrepancy is due to the fabrication tolerance which cannot be totally avoided. Concurrently, with these performances, the proposed antenna satisfies the requirements of WLAN/ WiMAX and C/X/Ku-Band applications.

Fig. 7. Fabricated prototype of the proposed antenna.
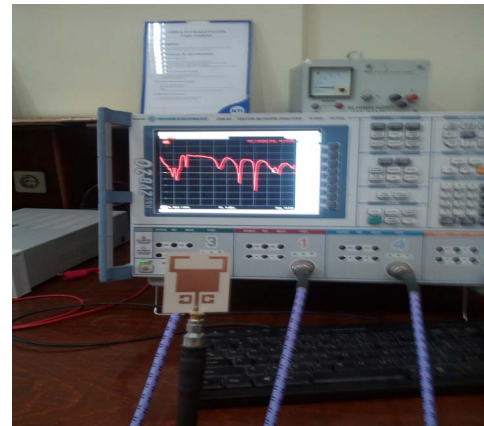
Fig. 8. Return loss of the proposed antenna using VNA.
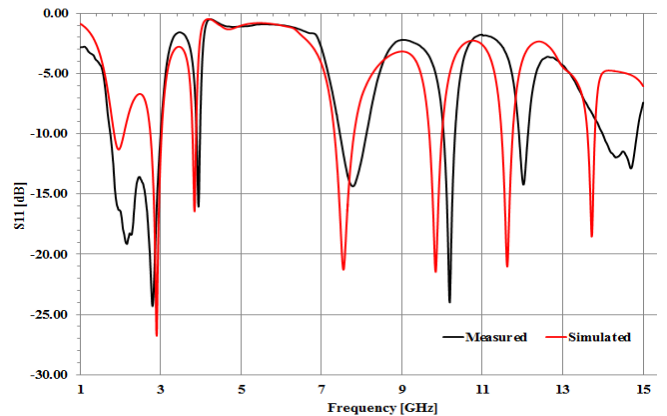
Fig. 9. Simulated and measured reflection coefficient of proposed tri-band antenna.

V.   CONCLUSION

A new compact monopole antenna with multi band features for wideband applications is presented in this work. The investigated topology operates at three different frequencies at at 7.58 GHz, 9.88 GHz, 11.59 GHz and 13.78 GHz. In order to improve the impedance bandwidth and radiation characteristics and to minimize the size of conventional rectangular antenna, stepped cuts at lower corners are added to the radiating patch and a partial ground plane has been etched on the metallic ground plane. The proposed antenna is simulated and manufactured on the FR4 substrate with an area

of 41.04 x 29.98 x 1.6 mm^3. The measured results show that the proposed topology operates at WLAN, WiMAX, C- (Uplink) X- (Uplink) and Ku- (Uplink) band applications. Simulation and measurement results show that the compact antenna due to its good characteristics can be a good candidate to be used in personal and mobile UWB applications. The appeared deviation between the simulation and measurement is assumed to be related to the mismatching at the SMA port and to the inaccurate of the fabrication. Taking into account the topic, comparisons between other similar antennas in aspects of size and design complexity have been made.

REFERENCES

[1] Yoon JH. Fabrication and measurement of modified Spiral-patch antenna for use as a triple-band (2.4 GHz/5 GHz) antenna. Microw Opt Technol Lett. 2006 Jul; 48(7):1275–9.

[2] Costantine J, Kabalan KY, El-Hajj A, Rammal M. New multiband microstrip antenna design for wireless communications. IEEE Trans Antennas Propag Mag. 2007 Dec; 49(6):181–6.

[3] Cobo L, Castro H, Quintero A. A location routing protocol based on smart antennas for wireless sensor networks. Indian Journal of Science and Technology. 2015 Jun; 8(11). Doi:10.17485/ijst/2015/v8i11/71788.

[4] Garg TK, Gupta SC, Pattnaik SS. Metamaterial loaded frequency tunable electrically small planar patch antenna. Indian Journal of Science and Technology. 2014 Jan; 7(11). Doi:10.17485/ijst/2014/v7i11/50178.

[5] Danideh A, Sadeghzadeh RA. CPW-fed slot antenna for mimo system applications. Indian Journal of Science and Technology. 2013 Jan; 6(1). Doi:10.17485/ijst/2013/v6i1/30557.

[6] Mehetre TR, Kumar R. Design of inscribed circle Apollo UWB fractal antenna with modified groundplane. Indian Journal of Science and Technology. 2012 Jun; 5(6):2846–50. Doi:10.17485/ijst/2012/v5i6/30474.

[7] Pourbagher M, Nourinia J, Pourmahmud N. Reconfigurable plasma antennas. Indian Journal of Science and Technology. 2012 Jun;5(6).Doi:10.17485/ijst/2012/v5i6/30487.

[8] Ghiyasvand M, Bakhtiari A, Sadeghzadeh RA. Novel microstrip patch antenna to use in 2×2 sub arrays for DBS Reception. Indian Journal of Science and Technology. 2012 Jul; 5(7): 2967–71. Doi:10.17485/ijst/2012/v5i7/30493.

[9] Okwara L, Kwaha BJ, Amalu P. Design and construction of array dipole antenna adaptable to VHF and UHF bands. Indian Journal of Science and Technology. 2011 Jul; 4(7). Doi:10.17485/ijst/2011/v4i7/30102.

[10] Kumar D, Pourush PKS. Yttrium ferrite based circularly polarized triangular patch array antenna. Indian Journal of Science and Technology. 2010 Apr; 3(4). Doi:10.17485/ijst/2010/v3i4/29733.

[11] Hindoliya DA, Jain JK. Performance of multistage evaporative cooling system for composite climate of India. Indian Journal of Science and Technology. 2010 Dec; 3(12). Doi:10.17485/ijst/2010/v3i12/29860.

[12] "High frequency structure simulator software package,"HFSS V13, Ansoft Corporation.

[13] A Boutejdar, M Amzi, SD Bennani, Design and Improvement of a Compact Bandpass Filter using DGS Technique for WLAN and WiMAX Applications. Telkomnika 15 (3), 2017

[14] A Boutejdar, M Challal, SD Bennani, F Mouhouche, K Djafri, Design and Fabrication of a Novel Quadruple-Band Monopole Antenna Using a U-DGS and Open-Loop-Ring Resonators, Advanced Electromagnetics 6 (3), 59-63, 2017

[15] A Boutejdar, W Abd Ellatif, A novel compact UWB monopole antenna with enhanced bandwidth using triangular defected microstrip structure and stepped cut technique, Microwave and Optical Technology Letters 58 (6), 1514-1519, 2016

[16] A Boutejdar, M Salamin, S El Hani, L Bellarbi, A Afyf, Compact Microstrip Antenna Covers WLAN, LTE, and WiMAX, Microwave & RF 50 (1), 13-17, 2017

[17] A Boutejdar, A Ibrahim, E Burte, Novel Microstrip Antenna Aims at UWB Applications, Microwaves & RF magazine 7 (7), 8-14, 2015

Physicochemical characterization of sodium bentonite clay and its significance as a catalyst in plastic wastes valorization

Awinash Kumar

Mechanical Engineering,

North Eastern Regional Institute of Science and Technology,

NERIST, Nirjuli, Itanagar,

Papumpare,

Arunachal Pradesh,

India-791109

Email: awinerist@gmail.com

(Corresponding author)

Pradip Lingfa

Mechanical Engineering,

North Eastern Regional Institute of Science and Technology,

NERIST, Nirjuli, Itanagar,

Papumpare,

Arunachal Pradesh,

India-791109

Email: pradip.lingfa@gmail.com

Abstract—This study reveals the physicochemical characterization and catalytic behavior of locally available sodium bentonite clay. The clay was treated with hydrochloric acid to identify the characteristics. This paper explains XRF, FT-IR, XRD, SEM, and TGA characterization of commercially available sodium bentonite clay, a potential catalyst for thermo- catalytic pyrolysis in waste plastic valorization. Phase identification, structural prop- erties, and chemical compositions were investigated. Less value of a loss on ignition (LOI) was found as 9.8% by weight which shows better acceptance performance for thermo- catalytic process of plastic wastes recycling. SiO_2 (52.55%), Al_2O_3 (15.34%), and Fe_2O_3 (11.92%) three major compounds were identified by XRF and satisfy the XRD pattern. Spectra show that at 1009.25 cm^{-1}, 1032.05 cm^{-1} and 1112.90 cm^{-1} band positions are strong bands of Si-O stretching of monosubstituted and tetrahedral compounds. Alcohols and phenols group of compounds have sharp band positions of H- O-H stretching at 3620.59 cm^{-1} and 3695.17 cm^{-1}. The maximum average crystallite size was found 26.55 nm for 25.09° (2Θ) absorption. The morphology indicates that the presences of large particles are in the form of agglomerates. The high weight percentage of SiO2 and CaCO3 were spotted respectively 45.40% and 42.18% by weight for raw clay in the scanning electron micrograph. After acid treatment, it was found that the % weight of $CaCO_3$ was decreased as 20.99% and % weight of SiO_2 was increased as 48.88%. Thermo gravimetric graph shows that the reliable temperature range is 450°C to 500°C, which satisfies the pyrolysis process temperature range. The objective of this paper is to explore the similar utilization of the montmorillonite group of clay as a catalyst and useful engineering aspects for recycling plastic wastes.

Index Terms—sodium bentonite, catalyst, physicochemical characteristics, pyrolysis, plastic wastes

I.   1. INTRODUCTION

Naturally occurring clay minerals such as bentonite, diatomite, smectite, kaolinite and fullers earth may be used as a substitute for activated carbon as an adsorbent, due to their good adsorption properties and low cost. There are two types of bentonite are found swelling type bentonite or sodium bentonite and non-swelling type bentonite or calcium ben- tonite. Most of the bentonite foun d worldwide is of calcium type [1-5] . Sodium bentonite is canonicalized compound, the bond donor count of hydrogen and bond acceptor of hydrogen count is 1 and 13 respecti vely. Bentonite is in the form of an aluminum phyllosilicate developed frequently from the conversion of volcanic ash, principally consists of smectite minerals, mainly montmorillonite (80-90 % by weight). When montmorillonite comes in contact with water can expand several times by its original volume. The offbeat characteristics of bentonite ; swelling, absorption/adsorption have increased their demand in different industries such as a binder, fillers of paper, nano -clays, catalyst, sealant, detoxifier, bleaching earth, pharmaceutical products, etc. The chemical structure varies with the type of water in which ash had fallen. Due to type and amount of impurities present, nature of exchangeable cations and the difference in the degree of chemical substitution of smectite structure the physical and chemical properties of clay minerals and clay deposits differ in nature. It is impossible for two or more deposits of the same clay minerals. Also, different clay samples from the same deposits have not the same chemical properties [6-7]. The common impurities in bentonite are calcite, feldspar, cristobalite, quartz, mica, ferrous carbonate and pyrite [8]. The deterioration temperature of sodium bentonite and calcium bentonite is about to 1180°F and 600°F respectively. The molecular weight of sodium bentonite is 422.286 g/mol and the reaction of cereal remains unaltered at temperature up to 900 ° F[9] .The present paper reveals the structural behavior of sodium bentonite by spec- troscopic method. The looking interest rationalizes for better applications of clays by the different instrumental techniques of characterization. The different types of physicochemical properties are calculated through FTIR, XRF, XRD, and SEM. The objective of this work is to demonstrate the chemical

composition, phase identification, and infrared spectrum of absorption or emission of sodium bentonite. It is essential to identify the behavior and adsorption capacity of clay samples in catalyzed reactions for better utilization. Change in infrared spectrum provides information on the mechanism as the difference of the spectra of nano -particles adsorbed on the surface of the clay. The physic-chemical properties are also calculated for further understanding of samples useful for the thermo- catalytic waste valorization of plastic wastes. The cost of the sodium bentonite clay is comparatively lower as compared   to the kaolin. A comparative analysis is done throughout the impurities present in the samples for an effective influence   of clays used as the catalyst in thermo- catalytic pyrolysis of waste plastics valorization.

II.   2. EXPERIMENTAL WORKS

2.1 Materials

Sodium bentonite belongs to the smectite group of clay has a similar structure of pyrophyllite. The clay used in this study was procured from Heilen Biopharm Pvt. Ltd, Gujrat, India. The composition of the sodium bentonite sample is as follows: 52.55% SiO_2, 15.34% Al_2O_3, 0.29% K_2O, 11.92% Fe_2O_3, 1.6% TiO_2, 2.75 % MgO, 1.4% CaO, 0.06% P_2O_5, 0.01% Cr_2O_3, 3.22% Na_2O, and 9.8% loss on ignition. Some impurities like quartz, mica, and feldspar are also present in the sample.

III. 2.2 CHARACTERIZATION TECHNIQUES

To determine the total volatile content (loss on ignition) 50 gm of clay sample was taken and by using muffle furnace   at the temperature 700°C for 1 hour the loss on ignition was calculated 9.8% for sodium bentonite. The sodium bentonite sample was characterized by X-Ray Fluorescence (XRF), X-Ray Diffraction (XRD) and Fourier Transformed Infrared Spectroscopy (FT-IR). The elemental analysis data of the clay samples were obtained through XRF PW2400 model of Phillips, scintillation detector having current 40 mA, voltage 40 mV, and rhodium anode X-ray tube. A Rigaku ULTIMA IV Powder X-Ray Diffractometer was used for XRD data collection with 2Θ measuring range -3° to 162°(maximum), minimum step size 0.0001°, goniometer radius of 285 mm, X-ray generator of maximum rated output 3 kW, rated tube voltage 20-60 kV, focus size 0.4 × 12 mm and employing Bragg-Brentano and parallel beam optics. The XRD pattern was obtained at room temperature in the range of 10° to 90°, with basic accuracy ±2°. X-ray of wavelength 1.540598 A°   is applied. FT-IR high-resolution data were collected by using a Model- SPECTRUM 100 of Perkin Elmer, auto-calibrated and traceable to AnC-38. The Model has accessories HATR (horizontal attenuated total reflection) and DRIFT (diffuse reflectance system). Data is recorded on K-Br pellets with a resolution of 4 cm^{-1} in the range of 450 cm^{-1} to 4000 cm^{-1} SEM analysis was recorded by LEO S430 scanning electron microscope attached with energy dispersive X-ray analyzer model OXFORD LINK ISIS. Model STD 2964 computerized TA machine was used for thermal analysis and α-Al_2O_3 was used as the reference material under atmospheric conditions.

IV. 3. RESULTS AND DISCUSSIONS

3.1 Loss on ignition test (LOI)

50 gm of each sample was taken for the loss on ignition test. Most of the researchers used the kaolin clay in alteration of plastic wastes to gain useful hydrocarbons tested for liquid transportation fuel. The pyrolysis technique was used by several for temperature ranges from 500°C to 800°C. The degradation process of plastic wastes besides with catalyst can be done to obtain high-quality products at low temperature [10]. Sodium bentonite has 9.8% LOI by weight. Muffle furnace was set on before doing a test for two hours to reach the temperature at 900°C. Kaolin clay sample and sodium bentonite samples of 50 gm were treated for 1 hour separately and weighed as 44 gm and 45.1 gm respectively by using electronic weight measuring instrument. This is done three times for separate parent clay samples. Less value of LOI for sodium bentonite shows that the acceptance performance as a catalyst using in waste plastic valorization is better than the kaolin clay. The pyrolysis technique was used by several for temperature ranges from 500°C to 800°C. The degradation process of plastic wastes besides with catalyst can be done to obtain high-quality products at low temperature [10]. Sodium bentonite has 9.8% LOI by weight.

3.2. X-ray Fluorescence Characterization

The XRF data of sodium bentonite shows that the base anhydride of sodium hydroxide Na_2O is richer than the kaolin sample, which is the useful sign for using as a catalyst in the waste valorization of plastics, has good tendency to enhance the pyrolysis process. Figure 1 shows the chemical compositions of high contents. Nickel (II) oxide is also traced which clarifies that the sodium bentonite has an important role in the pyrolysis process, however, Li et al. studied that the weight loss of biomass components occurred at low-temperature range and reduction in activation energy was observed. Also, Nano-NiO has a better catalytic effect than micro-NiO particles [11]. Table I represents the components of the sodium bentonite for the studied sample. The influence of CaO as a catalyst was studied by Investigations showed that the CaO plays an important role in pyrolysis for better outcomes [12-15]. The rich presence of CaO enhances the quality behaviour of sodium bentonite over clays. Existence of magnesium oxide is supporting the good catalytic behaviour of sodium bentonite in the pyrolysis reaction. [15-17].
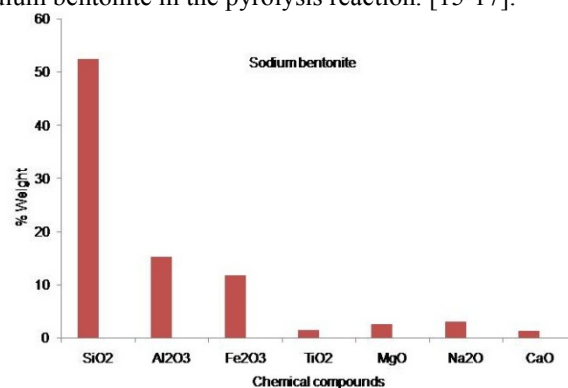

Figure 1.   Major chemical compounds present in the clay sample

TABLE I.
Compositions of Clay samples based on XRF (in weight (%))

Sodium bentonite	
Chemical compounds	%WEIGHT
SiO2	52.55
Al2O3	15.34
K2O	0.290
Fe2O3	11.92
TiO2	1.620
MgO	2.750
Na2O	3.220
CaO	1.400
P2O5	0.060
Cr2O3	0.010
NiO	0.020

3.3. FT-IR characterization of sodium bentonite

In this study from the IR spectra of the sodium bentonite, the absorption band at 3695.17 cm^{-1} is due to stretching vibration of O-H groups and relates to alcohols and phenol type of compounds shown in figure 2. A sharp band appears caused by the Si-O-H vibrations of photon energy.
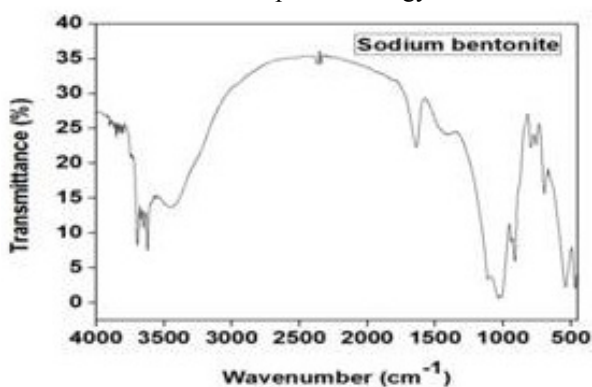

Figure 2.　FT-IR spectra of sodium bentonite clay

The band positions at 3445.87 cm^{-1} and 3620.59 cm^{-1} are due to H-O-H vibrations of water absorbed on the clay surface as well as vibrations of Si-O-H from the solid. Table 3 shows the IR band positions of the sodium bentonite due to different vibrations. The appearance of a band position at 796.59 cm^{-1} due to Al-Mg-OH stretching confirms the presence of quartz and has been confirmed by X-ray diffraction also. Two weak bands at 938.81 cm^{-1} and 1421.46 cm^{-1} are due to O-H bending of a carboxylic acid group and C-H bending of alkanes. A weak narrow band of 2380.24 cm^{-1} confirms the CO_2 group of compounds. Broad, strong broad and medium sharp bands of 698.49cm^{-1}, 539.26 cm^{-1}, and 470.79 cm^{-1} are due to Si-O, Si-O-Al, and Si-O-Si stretching.

3.4. X-Ray Diffraction Characterization of sodium bentonite clay

The absorption peaks found at 2Θ (°) = 5.71°, 7.61°, 12.55°,19.89°, 20.53°, 21.03°, 21.42°, 25.09°, 35.05°, 35.92°, and 61.69° shown by the IR spectra in figure 3. The maximum peak appears at 12.55°. Full Width at the half-maximum value (FWHM) is the same for the two absorption peaks at 5.71 A° and 7.61 A°. The average crystallite size (Dp) is maximum at 25.09° of absorption. The XRD pattern shows the presence of low quartz and silicon oxides at different absorptions which also

satisfy the XRF analysis. Triclinic (anorthic), monoclinic, cubic and orthorhombic crystal structures at different absorptions reveal the phase identification of the sample.
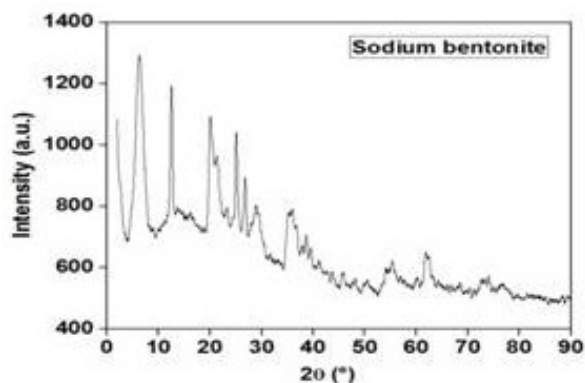

Figure 3.　XRD of sodium bentonite clay

3.5. Scanning electron microscopy (SEM) analysis of sodium bentonite

The morphological features have been reported in the scanning electron micrograph. The morphology indicates that the presences of large particles are in the form of agglomerates. More weight % of $CaCO_3$ and SiO_2 is spotted in spectrum 1 as shown in figure 4. The micrograph shows that flaky particles are stacked together. Broken edges are reported in the SEM image and a large number of clay particles are reported with Fe, Ti, Mg, and Al.
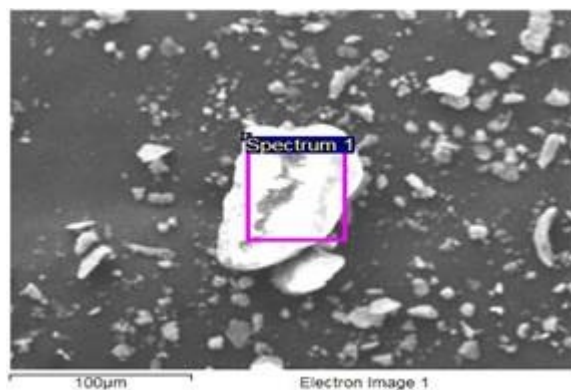
Figure 4.　SEM image of sodium bentonite

3.6 TGA and DSC (Differential scanning calorimetry) analysis of sodium bentonite

The thermo gravimetric curves for acid-treated sodium bentonite were depicted in figure 5. The initial sharp fall is due to the continuous loss of hydroxyl groups and hydration water at 110°C. The average degradation of sodium bentonite occurs between 400°C to 550°C. The curve shows that the negligible weight loss is above 650°C. The heat flow gradually increases up to 400°C and a sharp fall is recorded up to 800°C as recorded in figure 6. The glass transition occurs in between 0°C to 100°C and the crystallization range is 200°C to 400°C. The melting occurs about to after 450°C it satisfies the XRD results. The sodium bentonite is had more and more possibilities as a beneficial catalyst for the plastic waste pyrolysis process. As the pyrolysis is endothermic reaction occurs in the absence of oxygen the required heat flow is beneficial in case of sodium bentonite.

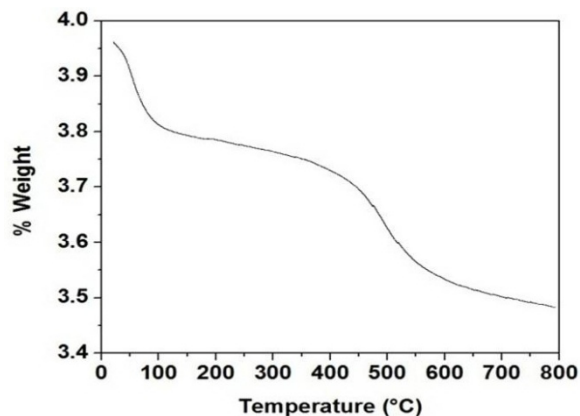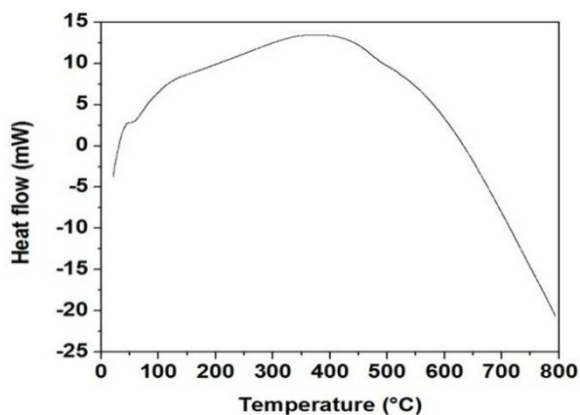Figure 5.   TGA graph of HCl treated sodium bentonite

Figure 6.   DSC graph of HCl treated sodium bentonite

V. 4. CONCLUSIONS

The analysis of sodium bentonite clay sample using XRF, FT-IR, XRD and SEM instruments have shown the prominent nature of the clay further useful as the alternate catalyst for plastic waste valorization. The commercially available clay is cheap and has better acceptable for the pyrolysis process. As the presence of alumina and silicate compositions are found from the XRF and the results of XRF supported by XRD, FT-IR and SEM analysis. Average crystallite size is found as 26.55 nm at the 25.09° of absorption, by XRD analysis. TGA and DSC curves satisfy the reliability required temperature range for useful waste plastic valorization using sodium bentonite as a catalyst.

References

[1] Asad, A., Shantanu, K., Mohammad, A.D. and Raquibul, H. (2013); Suitability of Bentonite Clay: An Analytical Approach. International Journal of Earth Science, 2(3): 88-95.

[2] Ahmed A.S, Salahudeen, N., Ajinomoh, C.S., Hamza, H. and Ohikere, A. (2012); Studies on the Mineral and Chemical Characteristics of Pindiga Bentonitic Clay. Petroleum Technology Development Journal (ISSN 1595-9104). An International Journal. 1: 1-8.

[3] Tijen, S. (2010); Purification and Modification of Bentonite and its use in Polypropylene and Linear Low-Density Polyethylene Matrix Nanocomposites. A PhD thesis submitted to the Chemical Engineering Department, Middle East Technical University.

[4] Ahonen, L., Korkeakoski, P., Tiljander, M., Kivikoski, H. and Rainer L.(2008); Quality Assurance of the Bentonite Material. POSIVA OY Working Report 33.

[5] RMRDC Raw Materials Research and Development Council (2007), Technical Brief on Mineral Raw Materials in Nigeria –Bentonite, Revised edn., Abuja.

[6] James O. O., Adediran, M. M., Adekola, F. A., Odebunmi, E. O. and Adekeye, J. I. D. (2008); Beneficiation and Characterisation of a Bentonite from North-Eastern Nigeria. Journal of the North Carolina Academy of Science, 124(4):154–158.

[7] Trauger, R.L (1994); The Structure, Properties and Analysis of Bentonite in Geosynthetic Clay Liners. Geosynthetic Resins, Formulation and Manufacturing. Proceedings of 8th GRI Conference.

[8] Holtzer, M., Bobrowski, A. and Grabowska, B. (2011); Montmorillonite: A Comparison of Methods for its Determination in Foundry Bentonites, Metabk 50(2):119-122.

[9] Vingas, G.J., Zrimsek, A.H., 1964. Thermal stability of bentonites in foundry moulding sand. In: Proceedings of the 13th National Conference on Clays and Clay Minerals, pp. 367–380.

[10] Miskolczi N, Bartha L, Deak Gy, Thermal degradation of polyethene and polystyrene from the packaging industry over different catalysts into fuel-like feedstocks, Polymer degradation and stability, 2006:517-526.

[11] Jianfen Li, Rong Yan, Bo Xiao, David Tee Lang, and Dong Ho Lee, Preparation of Nano-NiO particles and Evaluation of their Catalytic Activity in Pyrolyzing Biomass Components, Energy and fuels, vol.22:, Issue. 1,: pages 16-23, 2007.

[12] Wu, D., Zhang, S., Zheng, Q., Zheng, Q., Zhao, X., Liu, W., Xue, X., The influence of CaO on the Pyrolysis Behaviour and kinetic Characteristics of Low-Rank Coal., Energy Procedia, Volume 105,2017.

[13] Guan Rengui, Li Wen, Li Baoqing, Effects of Ca-based additives on pyrolysis of Datong coal [J], Journal of China University of Mining and Technology, 31 (4) (2002), pp. 396-401.

[14] Zhu Ting Yu, Lui Li Peng, Wang Yang, et al., Study on coal mild gasification with Cao catalyst [J], Journal of Fuel Chemistry & Technology, 2000,28(1): 36-39.

[15] Ersan Putin, Catalytic pyrolysis of biomass: Effect of pyrolysis temperature, sweeping gas flow rate and MgO catalyst, Article in Energy 35(7): 2761-2766, July 2010.

[16]S.A. Karakoulia, K.G. Kalogiannis, et al., Natural magnesium oxide (MgO) catalysts: A cost-effective sustainable alternative to acid zeolites for the in situ upgrading of biomass fast pyrolysis oil, Applied Catalysis B: Environmental, Volume, 196, 2016, pp. 155-173.

[17] Jungjaroenpanit C., Vitidsant T., Catalytic pyrolysis of used cooking oil by magnesium oxide supported on activated carbon in a continuous reactor, International journal of chemical Environmental and biological sciences, volume: 1 pp.429-432, 2013.

$Ni_{0.1}Co_{0.9}Fe_2O_4$ spinel ferrite as a promising magneto-dielectric substrate for X-band Microstrip Patch Antenna

Kunal Pubby
Department of Electronics Technology
Guru Nanak Dev University
Amritsar, India
kunalpubby02@gmail.com
Sukhleen Bindra Narang
Department of Electronics Technology
Guru Nanak Dev University
Amritsar, India
sukhleen2@yahoo.com

Sanjay R. Bhongale
Department of Physics
Yashavantrao Chavan Institute of
Science
Satara, India
sanjaybhongale@rocketmail.com

P.N. Vasambekar
Department of Electronics
Shivaji University
Kohlapur, India
pnv_eln@unishivaji.ac.in

Abstract— In the present study, the suitability of Ni-Co spinel ferrites as dielectric substrate for microstrip patch antenna has been reconnoitered in X-band frequency range. The scrutinized spinel ferrites with chemical composition $Ni_{1-x}Co_xFe_2O_4$ (x=0.00,0.30,0.60,0.90) were synthesized using Pechini's sol gel method. For the present study, Ansoft Designer SV2 was used to design and analyze the microstrip patch antenna. Simulation of antenna was done at resonant frequency of 10.02 GHz, which makes this research to find application in military and surveillance. Firstly, the antenna dimensions were calculated using resonant frequency and electromagnetic properties of the compositions. The antenna output parameters such as return loss, bandwidth, VSWR (Voltage Standing Wave Ratio), Smith Chart and radiation pattern were subsequently analyzed by the simulation Based on the analysis, Ni-Co ferrite $Ni_{0.1}Co_{0.9}Fe_2O_4$ has come out to be the best alternative out of the studied compositions for its possible usage as efficient dielectric substrate in microstrip patch antenna in 8.2 – 12.4 GHz frequency range.

Keywords— *Ni-Co spinel ferrite; microstrip patch antenna; X-band; VSWR; return loss; miniaturization.*

I. INTRODUCTION (*HEADING 1*)

Undoubtedly antennas are the electronic eyes and ears of today's world due to their indubitable place in communication technology. Any type of communication, whether wired or wireless, microwave or optical, involves antenna in one or another form. Antenna is basically a transducer which converts electrical signal to electromagnetic waves and vice-versa. It is an interface between transmitter/receiver and the channel. Its size and characteristics significantly affect the quality of service (QoS) of communication. In last few decades, the communication technology has grown exponentially. Therefore, antenna engineering needs to be reformed accordingly in order to cope up with the prevailing technology [1-2]. It is very interesting to note that lot of work has been done in the field of antenna. Different antennas such as parabolic reflectors, patch antenna, slot antenna, folded dipole antennas have been proposed for different applications. In this revolution of antenna engineering, microstrip patch antennas have emerged out as the most amazing development. These microstrip antennas have wide range of applications in microwave systems including radar, missiles, mobile & satellite communication, navigation, global positioning system (GPS) and biomedical systems, due to their lighter weight, low volume, low

production cost, simple planar structure, fabrication ease and conformity [1, 3-4]. These antennas have several technological advantages also such as dual-frequency operation, frequency agility, broad bandwidth, feedline flexibility and beam scanning omnidirectional patterning [5]. Microstrip patch antenna basically consists of a dielectric substrate sandwiched between a comparatively small sized conducting patch on one side and equal sized ground plane on the other side (Fig. 1). The conducting patch can be of any geometry, commonly of rectangular or circular shape [6-7]. Patch dimensions depend on the dielectric constant of substrate and the resonant frequency [8]. This antenna was initially proposed by G.A. Deschamps in 1953 [9], but was popularized by Robert E. Munson and his co-workers in 1970's [10]. Later on, different research groups scrutinized these antennas with different dielectric substrates [11-15].
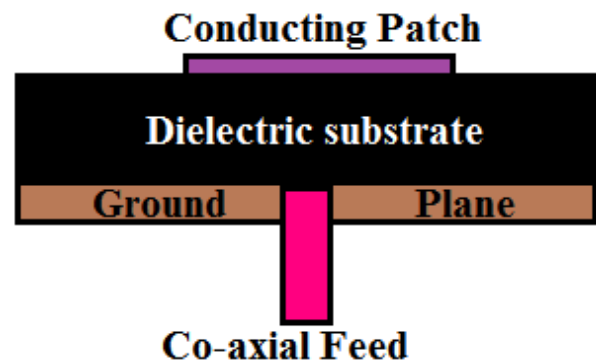

Fig. 1 Structure of Microstrip Patch Antenna

The role of dielectric substrate is very crucial in the design of microstrip antenna. Properties of antenna such as dimensions, efficiency, bandwidth and quality factor depend on the dielectric constant of dielectric material. The height of antenna can be miniaturized by factor $n = \sqrt{\mu_r \varepsilon_r}$ by use of suitable dielectric materials [1, 16]. The miniaturization factor n is also known as refractive index of the material [17]. But the miniaturization should not be done at the cost of compromise with the performance. High dielectric materials, a common choice for miniaturization, don't serve the purpose here as their usage also leads to degradation of pattern and radiation efficiency [12]. In this situation, materials with magneto-dielectric properties are required which allow both reduced antenna size and increased bandwidth [18-19]. Polycrystalline ferrites, having high electrical resistance, good chemical stability and mechanical

strength can be employed in these applications [20]. Among magneto-dielectric materials, spinel ferrites come out to be better choice in comparison to hexaferrites due to their lower sintering temperature and low production cost [21-22].

In the present work, Ni-Co spinel ferrites are scrutinized in X-band frequency range for their possible application in miniaturization of antenna. The reason behind choosing X-band for this study is that this band is a popular radar frequency sub-band used in civil, military, air traffic control, defense tracking, vehicle speed detection and weather monitoring applications. The samples under investigation were prepared using sol-gel auto-combustion route. The structural and X-band electromagnetic characterization of these samples has already been reported [23]. In this communication, the X-band complex permittivity and permeability values of the compositions was used to determine the antenna parameters. Then, the performance of the simulated antenna in terms of output parameters such as return loss, 10 dB bandwidth, VSWR, Gain, beam width and radiation pattern is analyzed in the frequency range 7 GHz to 13 GHz.

II. DESIGN PROCEDURE

A. Selection of the material for substrate

The material to be used for dielectric substrate must fulfill three essential conditions:

1. Resonant frequency of the antenna (f_r): f_r must lie within the limits of frequency band for which antenna is being designed. Since, the present antenna is simulated for X-band, hence the resonant frequency of material must lie between 8.2 GHz and 12.4 GHz. The resonant frequency selected for the present design is 10.02 GHz.

2. Permittivity (ε_r) and permeability (μ_r): Material with low permittivity is considered to be better for the design as it provides better efficiency, higher bandwidth, lower quality factor and high radiated power [24]. The use of magneto-dielectric material instead of pure dielectric material helps to minimize the size of antenna. In the present case, spinel ferrites with chemical formula $Ni_{1-x}Co_xFe_2O_4$ (x =0.0, 0.3, 0.6, 0.9) are used as magneto-dielectric substrate for the antenna. The electromagnetic properties, which are used for the simulation of antenna have already been reported elsewhere [23]. As reported in that research, all compositions have real part of permittivity in 5.14-5.69 range, making these spinel ferrites suitable for the antenna design.

3. Dielectric constant: Material with low dielectric constant is considered to be better for the design as it provides better efficiency, higher bandwidth, lower quality factor and high radiated power [24]. In the present case, four spinel ferrite compositions with chemical formula $Ni_{1-x}Co_xFe_2O_4$ (x =0.0, 0.3, 0.6, 0.9) are used as substrate for the antenna. All compositions have dielectric constant in 5.14-5.69 range, making them suitable for the antenna design.

4. Substrate thickness (h): Thick substrate increases the fringing field at patch periphery and increases the radiated power [24]. Also, the height of substrate with feed should lie in X-band frequencies. Hence, the height of substrate is chosen to be 2 mm.

B. Determination of patch dimensions (L_{pat} and W_{pat})

The rectangular microstrip patch antenna is designed by using selective four ferrite samples (NC 0.00, NC 0.30, NC 0.60 and NC 0.90) as substrate. The parameters required for design rectangular patch antenna such as are permittivity (ε_r), dielectric loss tangent (tan δ_e), permeability (μ_r) and magnetic loss tangent (tan δ_m) at operating frequency 10.02 were determined using Vector Network Analyzer (VNA) and are presented in Table 1 [23]. Using the values of ε_r and μ_r the length of antenna is determined by formula [25]: $L_{pat} = c/2f_r \sqrt{\mu_r \varepsilon_r}$, where c is the velocity of light in free space. The width (W_{pat}) of the antenna is optimized to suppress higher modes of excitation by simulation using Ansoft Designer SV2 [26].

C. Determination of substrate (L_{sub} and W_{sub}) and ground plane dimensions (L_g and W_g)

For practical considerations, it becomes necessary to have finite ground plane. The dimensions of substrate are equal to that of ground plane and are calculated using equations [27]: $L_{sub} = L_g = 6h + L_{pat}$ and $W_{sub} = W_g = 6h + W_{pat}$, where, h is the substrate thickness. The dimensions of patch are picturized in Fig. 2 and are listed in Table 1.
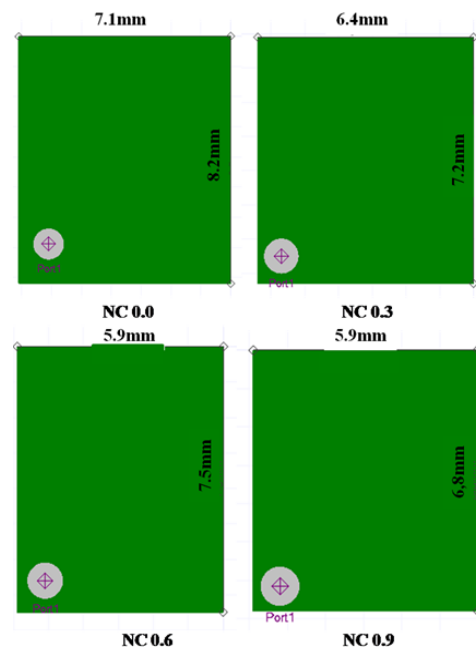

Fig. 2 Geometry of designed antenna

For feeding the microstrip antenna, there are several methods such as feed line, co-axial cable feed, probe feeding, aperture fed, proximity fed etc. But the most common is coaxial probe method due to its different advantages such as easy fabrication, better matching, low spurious radiation etc. The antenna, simulated in the present work, is excited by using coaxial feed technique. The feeding locations for impedance matching of 50 ohms with input impedance are optimized by rigorous trial and error method [28]. Thus the design input parameters of antenna such as permittivity (ε_r), dielectric loss tangent (tan δ_e), permeability (μ_r) and magnetic loss tangent (tan δ_m) at operating frequency 10.02 (f_r) are tabulated in Table 1.

TABLE I.   ELECTROMAGNETIC PARAMETERS AT RESONANT FREQUENCY, DIELECTRIC SUBSTRATE DIMENSIONS (L & W) AND COAXIAL FEED LOCATION FOR THE ANTENNAS SIMULATED USING SPINEL FERRITE COMPOSITIONS

Compos ition	f_r (GHz)	ε'	tan δ_e	μ'	tan δ_m	L mm	W mm	Feed Point
NC 0.00	10.02	5.14	0.052	0.851	0.121	7.1	8.2	-6.1, -6.9
NC 0.30	10.02	5.153	0.068	1.156	0.214	6.4	7.3	-5.7, -6.5
NC 0.60	10.02	5.444	0.07	1.186	0.136	5.9	7.4	-5.1, -6.6
NC 0.90	10.02	5.689	0.242	1.22	0.009	5.9	6.8	-5.2, -6.1

III. RESULTS AND DISCUSSION

The electromagnetic parameters of the spinel compositions at the resonant frequency 10.02 GHz have been tabulated in Table 1. These parameters for NC 0.90 composition are also plotted in Fig. 3 [23]. The spinel composition NC 00.90 has observed the highest value of permittivity and permeability at the resonant frequency of 10.02 GHz, which has made this composition to be capable of being simulated as the smallest antenna with dimensions 5.9 mm × 6.8 mm. These dimensions are in accordance to the formula provided in Eq. 1.
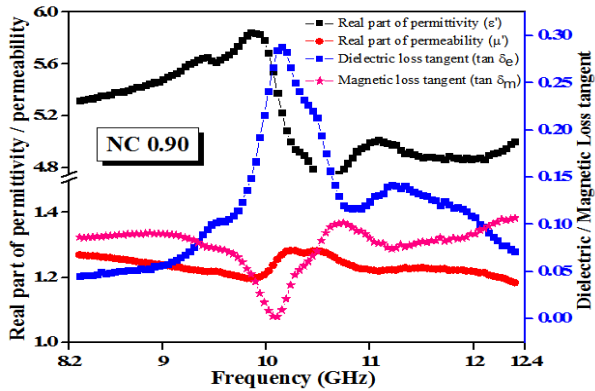

Fig. 3 Electromagnetic parameters of NC 0.90 composition in X-band

The value of miniaturization factor (n) are determined using the experimental values of permittivity (ε_r) and permeability (μ_r) using formula: n= $\sqrt{(\mu_r \varepsilon_r)}$. Its variation w.r.t. frequency for the prepared compositions in X-band is provided in Fig. 4. These values. It can be clearly seen that values of n for NC 0.00 is smaller in comparison to other three doped compositions. Values of n for NC 0.30, NC 0.60 and NC 0.90 lies in range 2.4 – 2.6 while that for NC 0.00 remains close to 2.
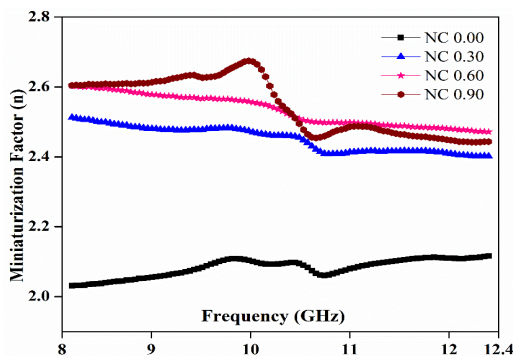

Fig. 4 Variation of miniaturization factor with frequency for ferrite compositions with frequency

The variation of simulated return loss with frequency is presented in Fig. 5. From this figure, it can be inferred that the designed antennas are resonant near the designed operating frequency of 10.02 GHz. The lowest return loss has been observed for the antenna on NC 00 ferrite substrate, owing to its better impedance matching obtained in this composition in comparison of other compositions. The % bandwidth for -10 dB return loss for antennas is provided in Table 2. The highest % bandwidth of 51.00 GHz is observed for an antenna on NC 0.90, whereas it is nearly equal for antennas on other ferrite substrates. The enhancement of bandwidth was also reported for Ni-Zn ferrites [10] and Cd – ferrite [13].
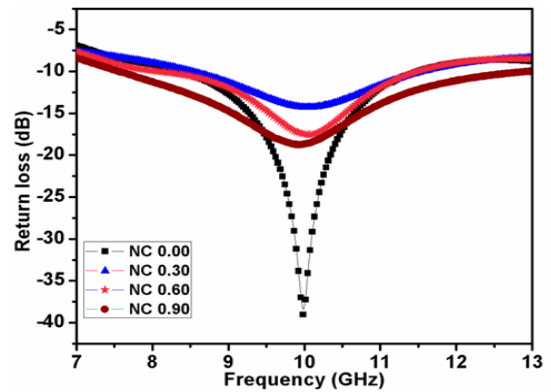

Fig. 5 Variation of simulated return loss with frequency.

TABLE II.   OUTPUT PARAMETERS: RETURN LOSS (R_L), % -10dB BANDWIDTH, VSWR, GAIN AND BEAM WIDTH OF THE SIMULATED ANTENNAS GOVERNING THE UTILITY OF THE SIMULATION

Compos ition	f_r (GHz)	R_L (dB)	% BW (GHz)	VSWR	Gain	Beam Width
NC 0.00	10.00	-39.50	28.58	1.027	0.67	88°
NC 0.30	10.08	-17.47	27.36	1.47	0.50	85°
NC 0.60	10.07	-14.20	30.33	1.31	0.55	88°
NC 0.90	9.94	-18.72	51.00	1.26	0.42	90°

The variation of voltage standing wave ratio (VSWR) with frequency in the range of 7 to 13 GHz is presented in Fig. 6. VSWR is a measure of how well the antenna is attached to the cables or how much power is reflected back into the cable. Ideally, value of VSWR should be 1. And in
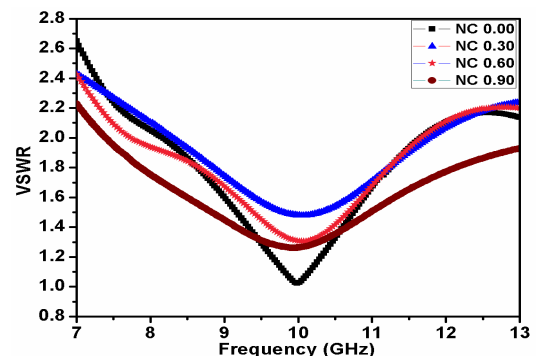

Fig. 6 Variation of simulated VSWR with frequency

our study, VSWR values for 4 compositions have been close to unity at operating frequency, which shows better optimization at feed location. The VSWR for NC 0.90 antenna has low value as compared to other doped compositions. Although the value of gain is minimum for

this composition, the highest beam width of 90° is achieved by this composition.

The Smith charts and radiation patterns of all antennas are analyzed by simulation. The characteristic Smith chart for antenna NC 0.00 and NC 0.90 are presented in Fig. 7, which shows the variation of impedance with frequency in the range of 7-13 GHz. From Fig. 7, it is seen that impedance shows only inductive loading throughout the range of 7-13 GHz. The reactive impedance of antenna simulated using NC 0.00 is nearly equal to normalized impedance over the studied frequency range. The VSWR at resonant frequency from smith chart is 1.027.
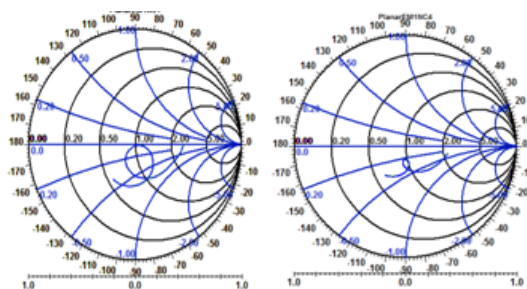

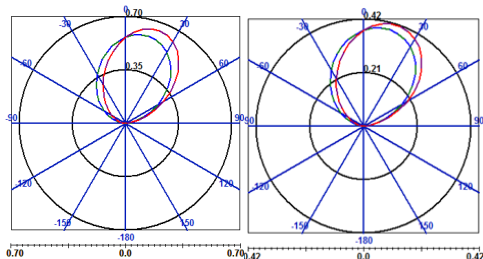Fig. 7 Characteristic Smith chart of antenna NC 0.00 and NC 0.90

Fig. 8 Representative Radiation pattern of antenna NC 0.00 and NC 0.90

The representative 2D polar radiation patterns of NC 0.00 and NC 0.90 are shown in Fig. 8. From radiation pattern, the values of maximum gain and beam width are calculated for all antennas and are tabulated in Table 2. The maximum gain (0.67) at operating frequency 10.02 GHz has been obtained for composition NC 0.00, while maximum beam width has been obtained for composition NC 0.90. The beam widths of all the antennas lie in 85°-90° range.

IV. CONCLUSION

The performance of microstrip patch antenna using Ni-Co spinel ferrites as dielectric substrate has been analyzed in X-band using Ansoft Designer SV 2.2. Using the electromagnetic properties, antenna dimensions have been determined. Antenna simulated using undoped composition has achieved the return loss of -39.5 dB. But the composition NC 0.90 has emerged as the best out of all the four compositions as it has got maximum -10 dB bandwidth % of 51%, maximum beam width of 90° and VSWR of 1.26. Also, the antenna fabricated using NC 0.90 has got minimum dimensions (5.9 mm $\times$ 6.8 mm) due to its favorable electromagnetic properties. Thus, this composition $Ni_{0.1}Co_{0.9}Fe_2O_4$ can be employed as a promising magneto-dielectric substrate for X-band Microstrip Patch Antenna where bandwidth is a primary issue and gain is a secondary issue.

REFERENCES

[1] K. Borah, N.S. Bhattacharyya, *IEEE Trans. Dielectr. Electr. Insul.* **17**, pp. 1676, 2010.

[2] N.K. Saxena, N. Kumar, P.K.S. Pourush, *Int. J. Radiol. Space Phys.* **40**, pp. 53 2011.

[3] K.M. Luk, C.L. Mak, Y.L. Chow, K.F. Lee, *Electron. Lett.* **34(15)**, pp. 1442-1443, 1998.

[4] S. Sukhija, K. Rakesh, A. Sarin, *Prog. Electromagnet. Res. M.* **62**, pp. 65-77, 2017.

[5] I. Singh, V.S. Tripathi, *Int. J. Comp. Tech. Appl.* **2(5)**, pp. 1595-1599, 2011.

[6] L.L. Basilio, M.A. Khayat, J.T. Williams, S.A. Long, *IEEE Trans. Antennas Propag.* **49**, pp.45-47, 2001.

[7] K. Alameddine, S.A. Chahine, M. Rammal, Z. Osman, *Int. J. Electron. Commun. (AEU)* **60**, pp. 596-598, 2006.

[8] M.A. Afridi, *Biological and Chemical Research*, vol. **2015**, pp. 128-132 Science Signpost Publishing.

[9] G.A. Deschamps, "Microstrip Patch Antenna", in *Third USAF symposium on Antennas*, 1953.

[10] A. Mehta, *Int. J. Sci. Tech. Res.* **4(3)**, pp. 54-57, 2015.

[11] M. Balaji, R.A. Jeyaram, P. Matheswaran, *J. Alloys Compd.* **696**, pp. 435 - 442, 2017.

[12] J.-L Mattei, L. Huitema, P. Queffelec, J.-F. Pintos, P. Minard, A. Sharahia, B. Jamnier, F. Ferrero, R. Staraj, D. Souriou, A. Thakur, *IEEE Trans on Magn* **47(10)**, pp. 3720-23, 2011.

[13] S.R. Bhongale, H. R. Ingavale, T. J. Shinde, P. N. Vasambekar, *J. Electron. Mater.* **47(1)**, pp. 577-584, 2018.

[14] X.M. Yang, Q.H. Sun, Y. Jing, Q. Cheng, X.Y. Zhou, H.W. Kong, T.J. Cui, *IEEE Trans. Antennas Propag.* **59(2)**, pp. 373-378, 2011.

[15] G. Li, H. Zhai, L. Li, C. Liang, R. Yu, S. Liu, *IEEE Trans. Antennas Propag.* **63(2)**, pp. 525-533, 2015.

[16] N. Das, S.K. Chowdhury, *IEEE Trans. Antennas Prop.* **AP 30**, pp. 499, 1982.

[17] R.C. Hansen, M. Burke, "Antenna with magneto-dielectrics", *Microw. Opt. Technol. Lett.* **26**, pp. 75-78, 2000

[18] A. Saini, P. Kumar, B. Ravelo, S. Lallechere, A.Thakur, P. Thakur, *Engg. Sci. Technol.: Int. J.* **19**, pp. 911-918, 2016.

[19] S. Bae, Y.K. Kong, A. Lyle, *J. Appl. Phys.* **103**, pp. 07E929, 2008.

[20] H. Anwar and A. Maqsood, *Electron. Mater. Lett.* **9**, pp. 641, 2013.

[21] L.B. Kong, Z.W. Li, G.Q. Lin, Y.B. Gan, *IEEE Trans. Magn.* **44**, pp. 559-565, 2008.

[22] D. Souriou, J.-L Mattei, A. Chevalier, P. Queffelec, *J. Appl. Phys.* **107(9)**, pp. 09A518, 2010.

[23] K. Pubby, S.S. Meena, S.M. Yusuf, S.B. Narang, *J. Magn. Magn. Mater.* **466**, pp. 430-445, 2018.

[24] A. Majumder, *Int. J. Engg. Trends Technol.* **4(4)**, pp. 1206-1210, 2013.

[25] C. A. Balanis, *Antenna Theory, Analysis and Design*, John Wiley & Sons. 3rd Edition, 2012.

[26] Ansoft Designer, www.ansoft.com.

[27] J. Huang, *IEEE Trans. Antennas Prop.* **AP-31(7)**, pp. 649-653, 1983.

A. Mandal, A. Ghosal, A. Majumdar, A. Ghosh, A. Das, S. K. Das, "Analysis of feeding techniques of rectangular microstrip antenna", in *2012 IEEE International Conference on Signal Processing, Communication and Computing (ICSPCC 2012)*, pp. 26-31 doi: 10.1109/ICSPCC.2012.6335619

Design and Simulation of Microstrip Antenna Using Composite Right/Left Handed Transmission Line (CRLH-TL) Technique for LTE and Radar Applications

Bishoy I. Halim[1]
Communications and Electronics Department,
Alexandria University
Alexandria, Egypt
gendibishoy@yahoo.com

Ahmed Boutejdar[2]
Microwave Engineering Department,
German Research Foundation (DFG)
Bonn, Germany
boutejdar69@gmail.com

Abstract— **A compact metamaterial inspired antenna operates at LTE and Radar applications is introduced in this paper.** Control and manipulation of electromagnetic waves is at the heart of many industries from wireless communication, internet and optical data storage to imaging and displays. Progress in these technologies places challenging demands on material properties and therefore structured electromagnetic materials. Metamaterials are a special class of structured materials. Patterning on the sub-wavelength scale allows precise engineering of their electromagnetic properties over a range going far beyond natural media. In this paper, microstrip antenna consists of radiating patch and two parasitic elements (open-loop ring resonators) to serve coupling bridges with partial ground plane and composite right / left-handed transmission line (CRLH-TL) embedded in the patch antenna. The antenna topology possesses an area $26 \times 37 \times 1.27$ mm³. The analysis and design is simulated and optimized commercial software. The good agreement between the theoretical expectation and the simulation results is observed. Finally, the proposed optimum antenna design structure has been fabricated and the measured *S*-parameters, VSWR of the proposed structure can be analyzed with network analyzer to demonstrate the excellent performance and meet the requirements for LTE and Radar applications.

Keywords— Microstrip antenna; CRLH-TL; LTE; Radar; Partial ground plane; Interdigital Capacitor; HFSS.

I. INTRODUCTION

In the present-time communication, antennas cover a wide range of applications in different areas, such as mobile communication, satellite navigation, internet services, automobiles and radars. Antennas are metallic structure which radiate and receive waves. Mobile phone handsets are generally required to be small in size. On mobile phone, current needed is more in terms of parameters such as shape, performances, qualities and its technology. There are various new technology arriving in wireless communication now a days that has brought a lot of devices which are portable in the future, such as a mobile phone that will possess function for fast data transmissions. LTE (Long Term Evolution) is the project related to high performance air interface for mobile telephony. LTE is the latest new technology that ensures competitive edge over existing standards: GSM, UMTS, etc. It improves user experience with full mobility. LTE minimizes the system and user-equipment complexities. LTE covers three bands, where the lower band includes frequency range of (698–966 MHz), middle band in the range of (1.427– 2.69 GHz) and higher band in the range of (3.4–3.8 GHz). Also, Radar has a wide range of applications in C-band (4-8 GHz) as well as X-band (8-12 GHz).

Metamaterials is a rapidly evolving field of research that covers a vast range of artificial structures and Electromagnetic properties. Resulting from this, there is no universally accepted definition of what is meant by a metamaterial [1-5]. It is generally agreed that metamaterials are artificial media with unusual properties not found in their constituent materials. In nature, the permittivity (ε) and the permeability (μ) of all the materials are positive. The Material with positive permittivity and permeability are referred as right-handed materials (RHMs). But the negative ε and μ can be achieved in some artificial materials, which are referred to as left-handed materials (LHMs). Metamaterials are periodic arrays of artificial structures with a pitch smaller than the wavelength of excitation. Due to their sub-wavelength periodicity, metamaterials do not diffract. Therefore, they appear homogeneous to an incident wave and can be described in terms of effective or averaged parameters that are controlled by the geometry of the metamaterial unit cell and its constituent materials. In analogy to natural materials, the elementary building block of a metamaterial, i.e. the metamaterial unit cell is often referred to as a metamolecule The CRLH metamaterials has been applied to some novel microwave devices [6-9]. The properties of the CRLH metamaterials can be analyzed by the transmission line theory.

The analysis and design of the proposed microstrip antenna supports multiband operations in much smaller size ($37 \times 26 \times 1.27 \ mm^3$). The structure of the antenna is very easy to fabricate. The proposed antenna has been successfully designed with Rogers RO3010 substrate by HFSS simulator [10]. An extensive analysis of the antenna parameters (reflection coefficient, gain, radiation pattern.) including surface current distribution is discussed in the following section. The good agreement between the simulation and

measured results are observed and the radiation characteristics have been illustrated the performance. Finally, the proposed design structure has been fabricated and the measured S- parameters in dB versus frequency in GHz, of the proposed antenna array structure can be analyzed with network analyzer.

II. THE CRLH-TL UNIT CELL

The proposed CRLH-TL unit cells structure have been designed using Rogers duroid 6010 substrate with (ε_r= 10.2, $tan\delta$ = 0.0023) and thickness of 1.27 mm. The interdigital capacitor and stub inductor provide the LH and also the RH contributions [11]-[12]. The top view of the proposed unit cells and its mechanical parameters in mm are shown in Fig.1. The characteristics of the proposed structure, such as simulated S_{11} in dB and the surface current density, J_{sur}, are obtained and analyzed for three different number of fingers, N = 7, 8 and 9 pair These analyses were done using HFSS simulator.

From Fig. 2, it was found that the RH capacitance is attributed to the capacitance between the trace and ground plane, and the RH inductance is caused by the magnetic flux generated by the current flow in the digits of the interdigital,

capacitor [6]. The proposed CRLH-TL unit cell structures have been achieved $S_{11} \leq$ -6 or -10 dB with multiband / wideband operational frequencies.
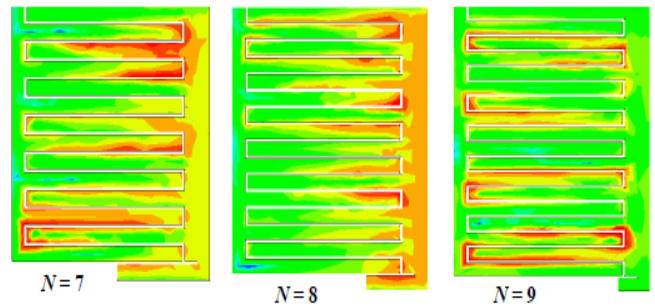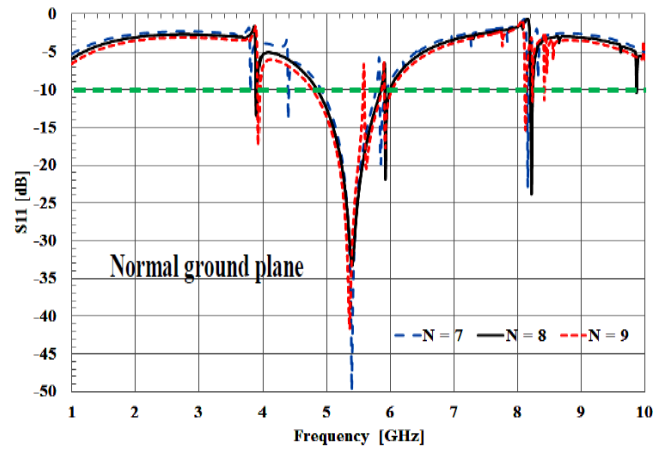

Fig. 2. The characteristics of the embedded proposed CRLH-TL Unit cell structures for N = 7, 8 and 9 fingers.

III. TWO UNIT CELL CRLH-TL

The proposed CRLH-TL with two unit cell elements array structure has been designed using Rogers duroid 6010 substrate. The top view of the proposed arrays structure and its mechanical parameters in mm are shown in Fig.3. The proposed CRLH-TL array structures have been achieved multiband/wideband operational frequencies with $S_{11} \leq$ -10 dB.

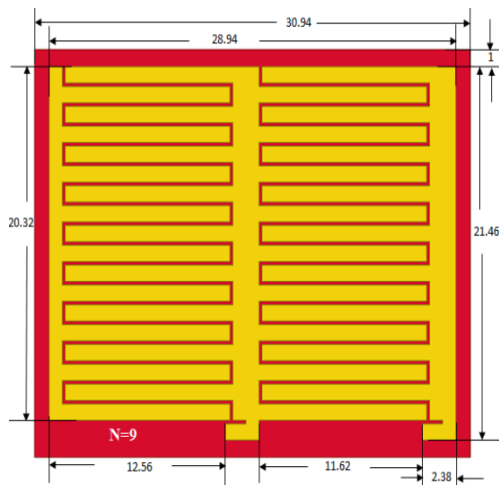Fig. 1. The proposed CRLH-TL unit cells structure for N =7, 8 and 9 fingers.
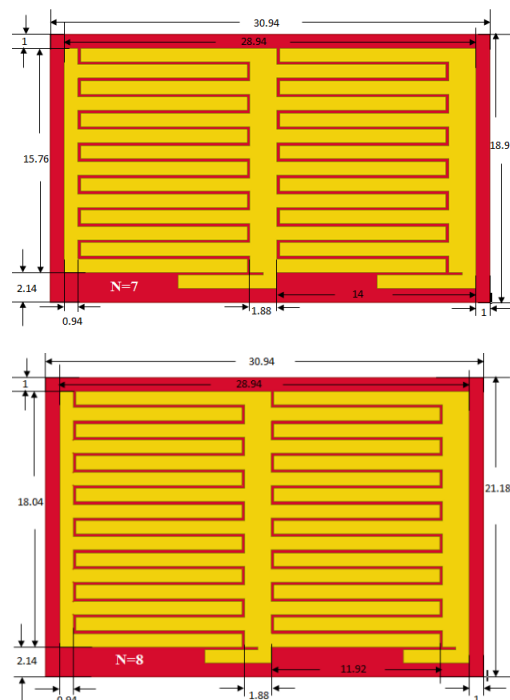
Fig. 3. The proposed CRLH-TL array structure for $N = 7$, 8 and 9 fingers.
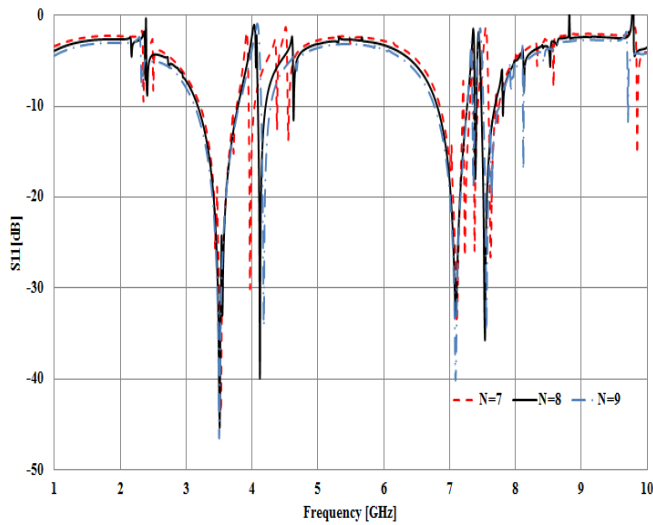

Fig. 4. The characteristics of the proposed CRLH-TL array structure with resonance frequency.

IV. MICROSTRIP ANTENNA DESIGN

A. Antenna Element without CRLH-TL Ground Plane

The structure of the proposed monopole multi-band antenna is shown in Fig.5. The design consists of a quasi-modified rectangular radiating patch with a partial ground plane [13]. The proposed rectangular antenna is fed by a 50 ohm microstrip line of width 1.2 mm and length 8.9 mm. The proposed monopole antenna is printed on a Rogers RO3010 substrate of thickness 1.27 mm, permittivity 10.2, and loss tangent tan δ = 0.0035. The overall dimension of the proposed antenna is only $37 \times 26 \times 1.27 \ mm^3$. A small partial ground plane slot has an area of only $8.9 \times 26 \ mm^2$ is etched from the ground plane to achieve multiband operation in compact dimension. The investigated antenna is connected to a 50 Ω-standard SMA connector to feed the microstrip line for RF signal input. All the parameters of the proposed antenna are finalized by parametric study through a number of simulations using HFSS software [10]. The simulated S_{11} in dB versus the frequency band 1-15 GHz and the surface current density have been shown in Fig.6 and Fig.7 respectively.
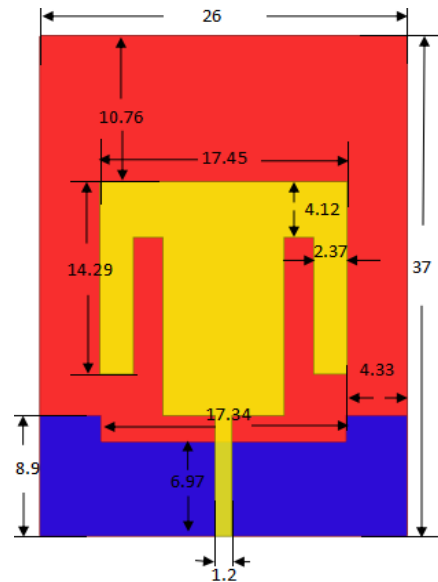

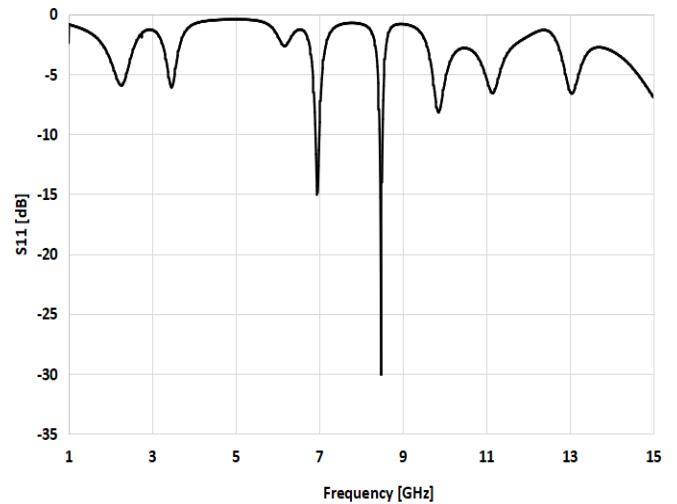Fig. 5. Geometry of the proposed antenna structure.

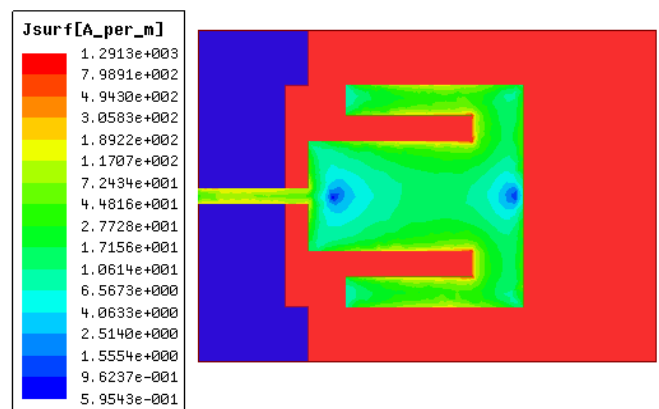Fig. 6. The simulated S_{11}[dB] of the proposed antenna without CRLH-TL ground plane.

Fig. 7. Surface current density, Jsur, of the proposed antenna.

B. Antenna Element with CRLH-TL Ground Plane

The proposed microstrip antenna with CRLH-TL structure embedded in the patch antenna at N=6 as an example has been introduced and analyzed. The proposed antenna is designed and fabricated on Rogers RO3010 substrate. The final top view of the proposed antenna is shown in Fig. 8. For the new performance of the final proposed antenna to achieve multiband operational frequencies, the position effect of the CRLH-TL structure has been understood compared with conventional antenna (without CRLH-TL array structure).
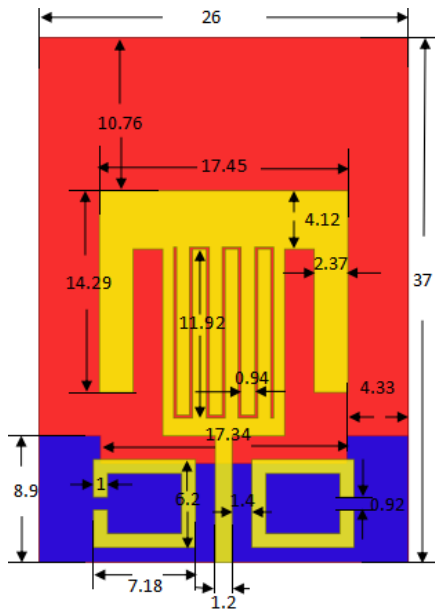

Fig. 8 The top, bottom views and mechanical parameters of the proposed antenna element with CRLH-TL on the top view.

V. SIMULATION RESULTS AND DISCUSSION

The simulated reflection coefficient curve of the proposed antenna is shown in Fig. 9. The simulated results indicate that the designed antenna achieves multiband operation with resonant frequencies.

It is observed from Fig. 10 that for operation, the surface current is mainly concentrated around the open loop ring resonators and thus increases the current path. So, the resonant frequencies are excited, generated and controlled by the parasitic open-loop resonators. The surface current distribution of the proposed antenna changes due to the presence of the open loop ring resonators that changes the resonance characteristics of the antenna. This is due to the fact that the distribution of electric and magnetic fields changes due to the lengthening of the surface current around the open loop resonators.

The simulated radiation patterns of the proposed monopole microstrip antenna with CRLH-TL is presented in Fig. 11. The proposed antenna shows almost stable radiation patterns with acceptable 3dB beam-widths.
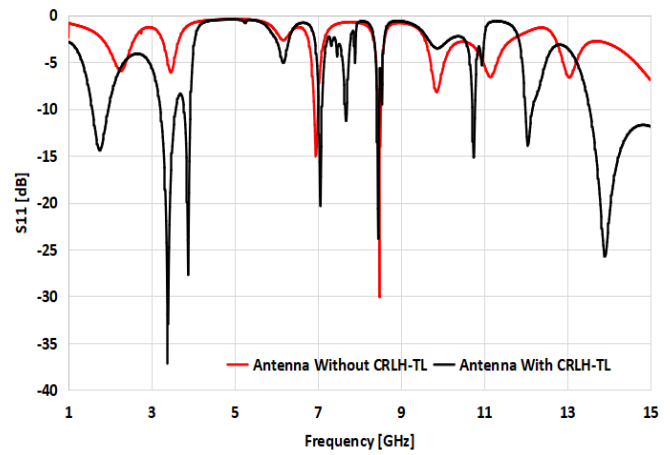

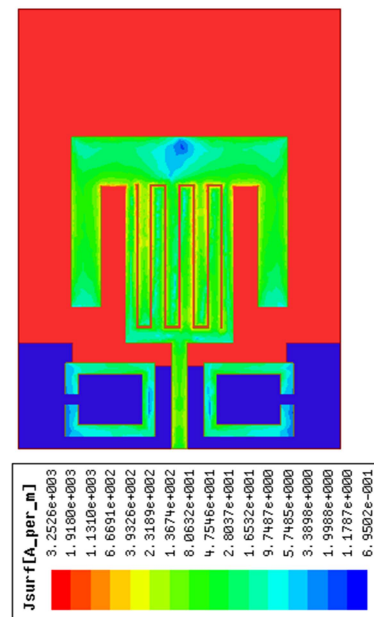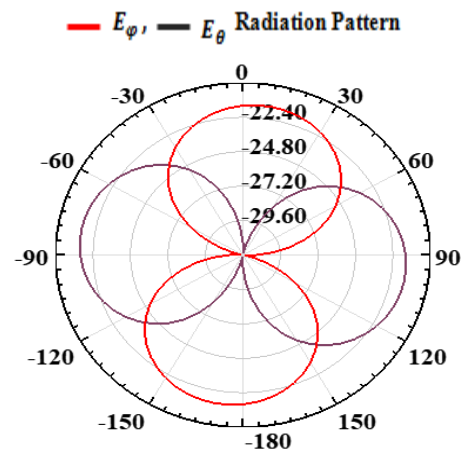Fig. 9. The simulated S_{11}[dB] of the proposed antenna with CRLH-TL ground plane.

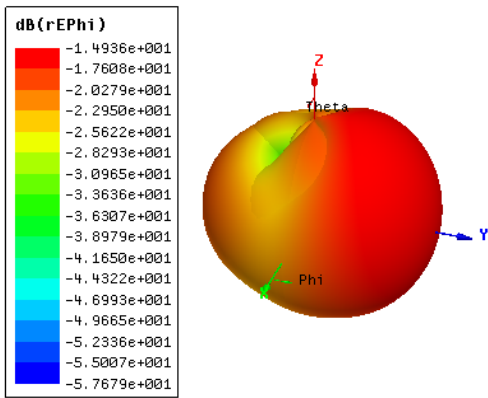Fig. 10. Surface current density, Jsur, of the proposed antenna with CRLH-TL ground plane.

Fig. 11 Simulated 2D radiation patterns of proposed antenna and 3D radiation pattern at 3.5 GHz.

VI. FABRICATION AND MEASUREMENT RESULTS

After the optimization of the proposed antenna parameters, an experimental prototype of the proposed design was fabricated using printed circuit technology and tested. A photograph of the fabricated antenna using printed circuit technology at antenna laboratory as shown in Fig. 12.
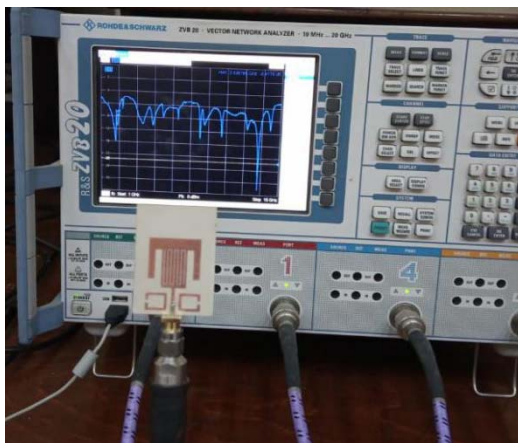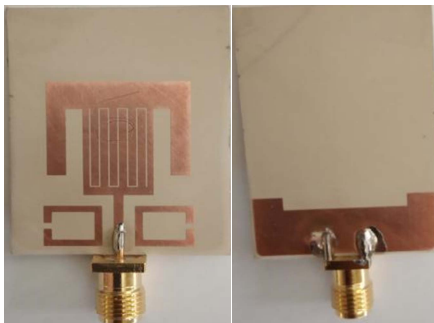

Fig.12. Fabricated prototype of the proposed antenna using VNA.

The measured S_{11} in dB of the proposed structure can be analyzed with network analyzer HP8719ES over a relatively wide frequency range from $1-15$ GHz as shown in Fig. 13. The measured VSWR of the proposed antenna is shown in Fig. 14. The measured values of the voltage standing wave ratios of the proposed antenna lie within 2:1 for all of the operating resonant frequencies, which indicates less reflected power and better impedance matching.
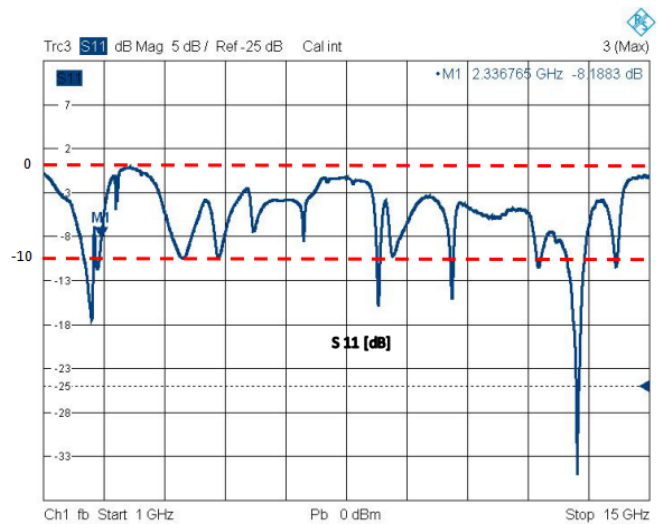

Fig. 13. The measured reflection coefficient of the proposed antenna.
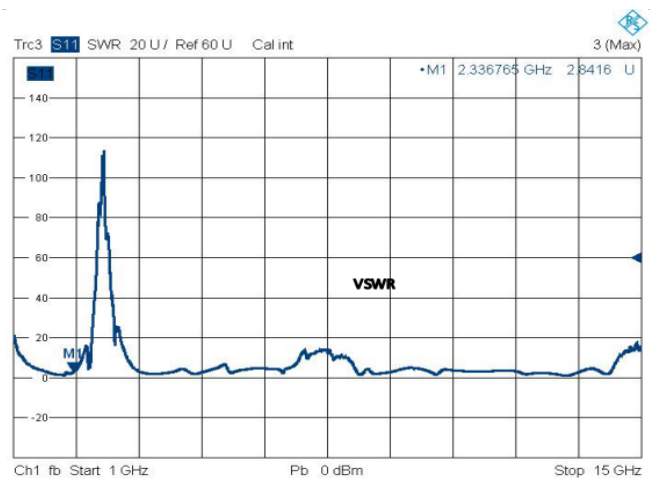

Fig.14. The measured VSWR of the proposed antenna

VII. CONCLUSION

An advanced and cost-effective multiband antenna for LTE, Radar, applications is designed, fabricated and tested. Antenna miniaturization is obtained by introducing CRLH-TL structure over the RO 3010 substrate which provokes multiband frequency characteristics by increasing the number of resonant frequencies without modifying the dimensions of the square patch antenna. The proposed antenna design has simple structure and can be used in multiband communication systems.

REFERENCES

[1] A. Sihvola, "Metamaterials in electromagnetics," Metamaterials, 2007.

[2] N. Engheta, "Meta-electromagnetics and meta-optics," Electromagnetic Theory (EMTS), Proceedings of 2013 URSI International Symposium on , vol., no., pp.1,2, 20-24 May 2013.

[3] M. A. Eberspacher and T. F. Eibert,"An analysis and design procedure for composite right/left-handed unit cells," 6th European Conference on Antennas and Propagation (EUCAP), pp. 1391–1394, April 2011.

[4] W. Cao, B. Zhang, A. Liu, T. Yu, D. Guo, and X. Pan,"Multi- frequency and dual-mode patch antenna based on electromagnetic band-gap (EBG) structure," IEEE Transactions on Antennas and Propagation, vol. 60, no. 12, pp. 6007–6012, December 2012.

[5]   Chang K., Qi T., and Xin H, "Balanced and symmetric design of active composite right- / left-handed transmission line with gain," Microwave Symposium Digest (MTT), 2012 IEEE MTT-S Inter., pp.1,3, June 2012.

[6]   I. A. Mocanu, G. I. Sajin, and F. Craciunoiu,"Electromagnetic study of strong coupled CRLH transmission lines for use in antenna construction," 2012 IEEE Asia-Pacific Conference on Antennas and Propagation, Singapore, August 2012.

[7]   E. David, and Y. Yoon,"Bridged composite right/left handed unit cell with all-pass and triple band response," IEEE Microwave and Wireless Components Letters, vol. 22, no. 11, pp. 568–570, November 2012.

[8]   X. L. Sun, J. Zhang, S.W. Cheung and T.I. Yuk," A small patch antenna using a single CRLH TL unit Cell," Radio and Wireless Symposium (RWS), 2012 IEEE , vol., no., pp.299,302, 15-18 January 2012.

[9]   Z. Wang, B. Li, C. Cao, M. Wu, L. Peng,"A compact multi-band antenna based on metamaterial," Microwave and Millimeter Wave Technology (ICMMT), Inter. Conf. on , vol.2, pp.1,4, 5-8 May 2012.

[10]   "High frequency structure simulator software package," HFSS V13, Ansoft Corporation.

[11]   Y. M. Madany, D. M. Abd-Elaziz and B. I. Halim, "Robust analysis and investigation of multiband composite right / left handed transmission line (CRLH-TL) for wireless band applications" International Conference on Electromagnetics in Advanced Applications (ICEAA), Italy, September 2013.

[12]   M. A. Othman, A. D. Alwakil, M. Shafee, T. M. Abuelfadl, A. M. E. Safwat, "Novel Even/Odd Mode-Based CRLH Unit Cells," Microwave Symposium Digest (MTT), IEEE MTT-S Inter., pp.1-3, June 2012.

[13]   Ahmed boutejgar, Bishoy I. Halim. "Design and Investigation of Rectangular Microstrip Patch Antenna Using Two Resonators and Partial Ground Plane for Multiband Applications" Computer Science and Electronic Engineering Conference (CEEC), UK, September 2018.

Design of 1-bit Full Adder using output wired CMOS Inverter based Threshold Gate

Mili Sarkar, G. S. Taki

Electronics and Communication Engineering Institute of
Engineering and Management Kolkata, India
Milisarkar777@yahoo.co.in, gstaki@iemcal.com

Abstract—**A new implementation technique of 1-bit Full Adder using output wired CMOS inverter based threshold logic is presented. With the advancement of nano technology threshold gate based logic design has got a new direction. In this paper first carry output is designed using output wired CMOS inverter based majority gate. Then Sum output is designed using Threshold gate. The number of transistor is less than the CMOS based Full Adder Circuit. The major advantage of this CMOS Threshold gate is it's simplicity. It's delay time is only around three inverter delays. The proposed design has been verified by means of simulation using PSPICE.**

Keywords— *Adder; Threshold Logic (TL) Gates; Majority gate; Complementary Metal Oxide Semiconductor (CMOS).*

I.INTRODUCTION

In this paper we propose a novel full adder cell which is a key component in all kinds of computing systems. The adder cell is based on linear threshold logic and majority gate [1]. There are several issues related to the full adders. Some of them are power consumption, performance, area, noise immunity and regularity and good driving ability [2]. Several works have been done in order to decrease transistor count and consequently decrease power consumption and area [3, 4, 5].

In Integrated Circuits mainly two types of full adders (Static & dynamic) are used. Static full adders commonly are more reliable, simpler .In this paper a static design of Full Adder is proposed. Threshold logic (TL) was introduced over six decades ago. There are many theoretical results showing that TL circuits are more powerful than classical Boolean circuits. It also offers much larger fan-in in comparison with the conventional logic gates [6]. A logical function which is linearly separable can be designed using threshold logic. However different TL gate realizations are made in recent papers [7,8,9 10,11,12].

The remainder of this paper is organized as follows:
SectionII: Describes the concept of threshold logic.

Section III: Describes the concept of majority gate.
SectionIV: Describes output wired CMOS inverter based threshold and majority gate
SectionV: Investigates the output wired CMOS inverter based one bit Full-Adder and its output waveforms.
Section VI: Gives the conclusion of the whole experiment

II. The concept of Threshold Logic

A linear threshold gate (LTG) is an n binary input and one binary output function [13].
Threshold Logic Gates are able to compute any linearly separable Boolean function given by-

$$Y= \text{sgn}\{F(x)\} = 0, \text{ if } F(x) <0$$
$$1, \text{ if } F(x) \geq 0 \qquad (1)$$
$$F(x) = \sum w_i x_i - \psi \qquad (2)$$

Where x_i is the n Boolean inputs and w_i is the corresponding n integer weights. The LTG compares the weighted sum of inputs and the threshold value ψ. If the weighted sum of inputs is greater than or equal to the threshold, the gate produces logic 1. Otherwise, the output is logic 0.
The basic Boolean logic functions AND,OR,NAND,NOR and NOT can be represented in the form of (1) and (2) as follows:

$$AND(x1, x2) = \text{sgn}\{ x1+ x2-1.5\} \qquad (3)$$

$$OR(x1, x2) = \text{sgn}\{ x1+ x2-0.5\} \qquad (4)$$

$$NAND(x1, x2) = \text{sgn}\{- x1- x2+1.5\} \qquad (5)$$

$$NOR(x1, x2) = \text{sgn}\{- x1- x2+0.5\} \qquad (6)$$

$$NOT (x1) = \text{sgn}\{- x1+0.5\} \qquad (7)$$

These basic logic functions can be designed with threshold gate as shown in figure 1.

In this diagram AND gate is designed. Other gates can be also designed by changing the weights and threshold values.
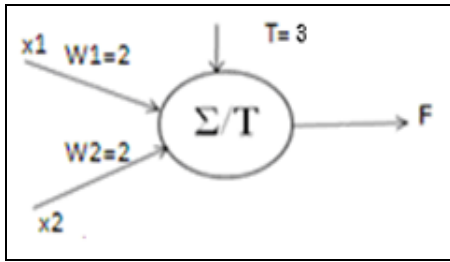

Figure 1: Design of Threshold logic based AND gate

III. THE CONCEPT OF MAJORITY GATE

The majority gate gives the logic output 1 when the number of one is more than the number of zeros at the input side. As for example OR gate is a Majority Gate. It is a special application of threshold logic. The majority gate can be designed using ganged output wired inverter circuit. [14]

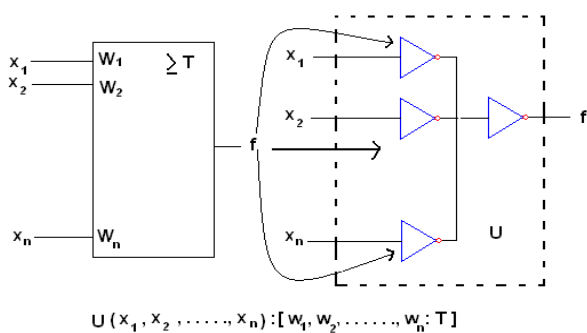### IV. OUTPUT WIRED CMOS INVERTER BASED THRESHOLD AND MAJORITY GATE

Figure2: Nonstandard symbol of Threshold gate and threshold gate basic structure using output wired ganged CMOS .

Figure 2 shows the nonstandard symbol for threshold gate and threshold gate basic structure using output wired ganged CMOS [15,16, 17]. Each input x_t drives one inverter, all inverter outputs are shorted together to design a nonlinear voltage divider which drives the output inverter whose purpose is to quantize the nonbinary signal at the ganged output node .The length of all the PMOS and NMOS transistors of

inverters are same. The PMOS and NMOS transistor widths of each inverter are designed depending on the weight (W) and threshold value(T) to be implemented. The weight values other than 1 can be realized by changing the width of the PMOS transistor. Thus, the design process involves sizing only two inverters the basic input inverters and the output inverter.
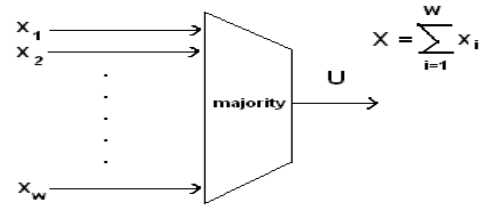A binary majority gate shown in fig3.

Figure 3: Function of majority gates

Here, w is the number of inputs which is usually odd. The output will be '1' if the number of '1's in the input side is more than the number of zeros.

A majority function is a special case of a threshold logic gate when the T is equal to (w+1)/2. The majority gate design based on ganged CMOS shown in Figure 4.
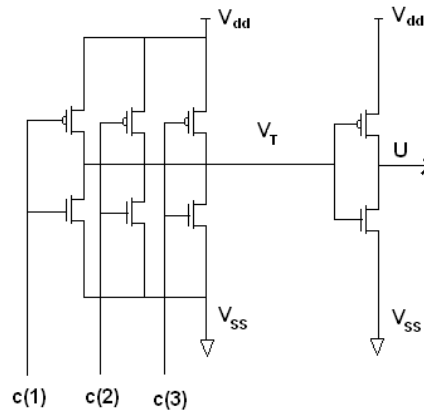

Figure4: Circuit of three input majority gate

It is made up of two parts: a nonlinear voltage divider made up of output wired inverters on the left hand side and an inverting buffer which senses the majority transition and provides a positive output on the right. The output inverting buffer isolates the divider output node from external circuitry to reduce noise effect and driving from the next stage. It also reshapes the output waveforms.

V. DESIGN OF ONE BIT FULL ADDER USING OUTPUT WIRED CMOS INVERTER BASED THRESHOLD AND MAJORITY GATE

Here we have used one majority gate and one threshold gate to implement a full adder circuit. The threshold gate based implementation of full adder and the equivalent output wired ganged CMOS based one bit Full Adder circuit are shown in figure5 and figure 6. [18]
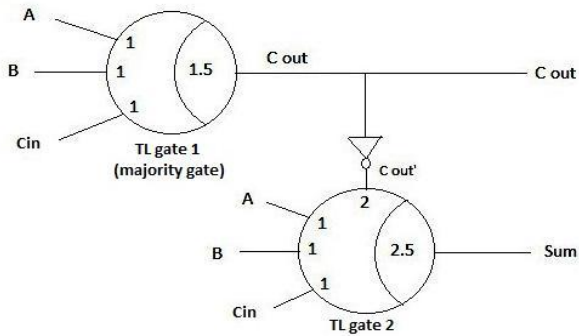

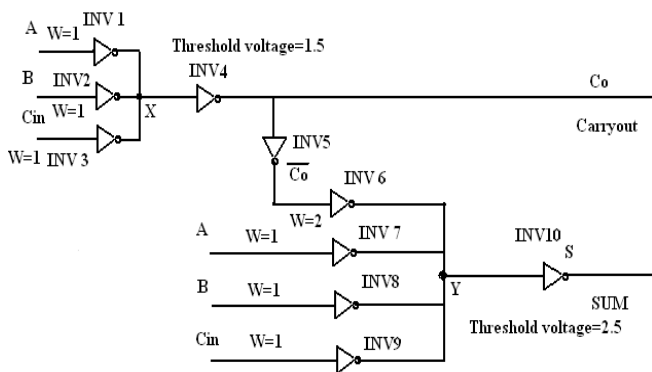Figure5:Threshold Logic gate based Full Adder Circuit.

Figure 6: Output wired ganged CMOS based one bit Full Adder circuit

Here two threshold gates are used TL gate1 and TL gate2.TL gate1 gives the carry output and it is a majority gate.This Majority gate is designed using four inverters. Three of them are ganged and from that ganged output, the fourth inverter is connected to get the carry output. Inputs of full adder (A,B,Cin) are applied to three inverters(INV1,INV2,INV3) which is shown in figure 6. The W/L ratio of all the PMOS and NMOS transistors are chosen such that the resistance of all the transistors are equal (R).So The equivalent circuit of ganged part may be considered as a voltage divider network. Ganged output voltage at node X is

calculated as a fraction of V_{dd} as shown in the following table.

A	B	Cin	Ganged output voltage(Vx)	Equivalent voltage divider network
1	1	1	0	
1	1	0	Vdd/3	
1	0	1		
0	1	1		
1	0	0	2(Vdd/3)	
0	1	0		
0	0	1		
0	0	0	3 (Vdd/3)	

Table1:Ganged output voltage and its equivalent voltage divider network for different input combinations of majority gate(TL1).

According to this the threshold voltage of the last output inverter is set in between $V_{dd}/3$ and $2(V_{dd}/3)$. The last inverter gives the carry output.

Carry output is taken and inverted by another inverter(INV5). Ultimately this is used as a fourth input for the TL gate 2 which will give sum output.

INV6,INV7, INV8 and INV9 form the ganged CMOS for this threshold logic.For INV7,INV8,INV9 the weight is 1 so the resistances for PMOS and NMOS transistors of these inverters are same which is R. For Inverter6 the resistance of PMOS transistor will be R/2 which is adjusted by the W/L ratio of that transistor to achieve weight 2. The ganged output Voltage at node Y is calculated from the equivalent voltage divider network which is shown in the following table. The equivalent Voltage divider circuit is shown in figure7.

A	B	Cin	Co	Co'	Vy	S
0	0	0	0	1	3/4Vdd	0
0	0	1	0	1	1/2 Vdd	1
0	1	0	0	1	1/2 Vdd	1
0	1	1	1	0	3/5 Vdd	0
1	0	0	0	1	1/2 Vdd	1
1	0	1	1	0	3/5 Vdd	0
1	1	0	1	0	3/5 Vdd	0
1	1	1	1	0	2/5 Vdd	1

Table2: Ganged output voltage for TL2
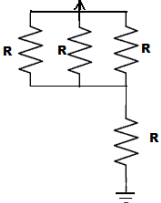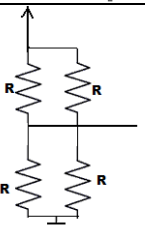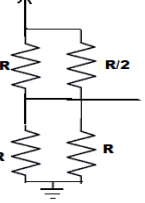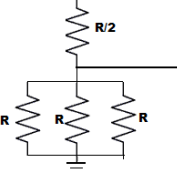
A	B	Cin	Co'	Equivalent voltage divider network
0	0	0	1	
0 0 1	0 1 0	1 0 0	1 1 1	
0 1 1	1 0 1	1 1 0	0 0 0	
1	1	1	0	

Figure7: Equivalent voltage divider network

From table 2 it can be concluded that the threshold voltage of the last inverter (INV10) should be in between 3/5 V_{dd} and 1/2 V_{dd}. According to this the last inverter is designed by adjusting the W/L ratio of the PMOS and NMOS transistors of it.

The circuit is simulated using PSPICE for 80ns.The 8 different input combinations exist for 10ns each. The supply voltage(V_{dd}) is taken as 3.3 V.The output

waveforms are shown in figure 8.Upper one is for Sum output and lower one is for Carry Output.
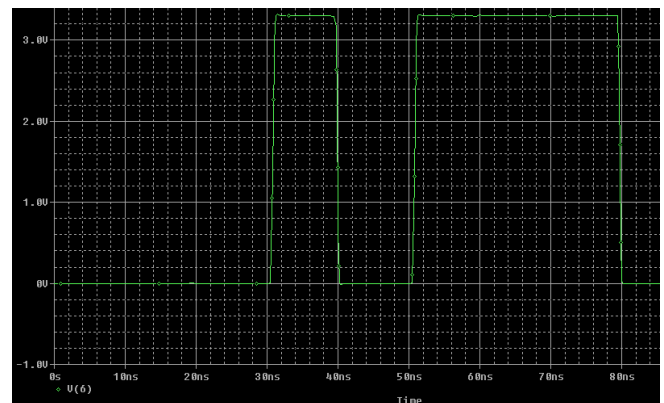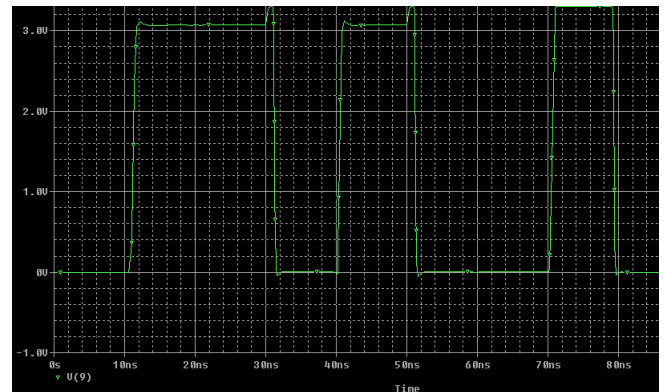

Figure 8: Sum and Carry output waveforms.

The total delay of the circuit is only five inverter delay which is almost 1ns measured for different models of transistor used.

VI.CONCLUSION

In this paper, we proposed the output wired CMOS inverter based one bit Full Adder circuit. The number of transistors required for this design is twenty.The total power consumption is 7.04E-04watts.

REFERENCES

[1] A Threshold Logic Full Adder Based on Resonant Tunneling Transistors, published at: ESSCIRC'98

[2] R. Shalem, E. John, and L. K. John, "A novel low-power energy recovery full adder cell," in *Proc. Great Lakes Symp. VLSI*, Feb. 1999, pp. 380–383

[3] H. T. Bui, Y. Wang, and Y. Jiang, *"Design and Analysis of 10- Transistor Full Adders Using XOR-XNOR Gates,"* IEEE Trans. Circuits and Syst. II, Analog Digit. Signal Process., vol 49, no. 1, pp. 25-30, Jan. 2002.

[4] K. Navi, M. Maeen, V. Foroutan, S. Timarchi, and O. Kavei, *"A Novel Low Power Full-Adder Cell for Low Voltage,"* Integration the VLSI Journal, 2009

[5] S. Veeramachaneni, M. B. Sirinivas, *"New Improved 1-Bit Full Adder Cells",*CCECE/CGEI, Canada, 2008

[6] P.K. Sinha Roy,'' Test & realization of linearly separable switching functions'', Int. J. Control, 1970, Vol.11, No.5, 873-89

[7] T. Shibata and T. Ohmi, "An intelligent MOS transistor featuring gate-level weighted sum and threshold operations," in *IEDM, Technical Digest*, New York, NY, USA, Dec 1991, IEEE.

[8] H. O¨ zdemir, A. Kepkep, B. Pamir, Y. Leblebici, and U. C¸ iliniroˇglu, "A capacitive threshold-logic gate," *IEEE JSSC*, vol. 31, no. 8, pp. 1141–1149, August 1996.

[9] P. Celinski, J. F. L´opez, S. Al-Sarawi, and D. Abbott, "Low power, high speed, charge recycling CMOS threshold logic gate," *IEE Electronics Letters*, vol. 37, no. 17, pp. 1067–1069, August 2001.

[10] Mili Sarkar Sunit Das Upasana Roy Chowdhury Dibyajyoti Das " Design of Sequential Circuits using Single Electron Encoded Logic"IEMCON 2012**.**

[11] Mili Sarkar, Shilpi Raj,Prasenjit Sengupta "Design of Sequential circuits using Threshold Logic"S. Muroga, *Threshold Logic and Its Applications*. New York: Wiley,197

[12] 'Bit-sliced median filter design based on majority gate'- C.L.Lee, C.W.Jen Dec. 1995. K. Elissa, "Title of paper if known," unpublished.

[13] M.J. Avedillo, J.M. Quintana, A. Rueda, and E. Jim´enez, "Low-power CMOS threshold-logic gate," *IEE Electronics Letters*, vol. 31, no. 25, pp. 2157–2159,

[14] J. Fernandez Ramos, J. A. Hidalgo Lopez, M. J. Martin, J. C. Tejero, and A. Gago, "A threshold logic gate based on clocked coupled inverters," *International Journal of Electronics*, vol. 84, no. 4, pp. 371–382, 2001.

[15] Y Taur , D.A. Buchanan, W. Chen , D. Frank, K. Ismail, H. Wann,S. Wind, and H. Wong. CMOS Scaling into the Nanometre Regime. Proceeding of the IEEE, Vol. 85(No.4):pp.486-504, 1997.

[16] IEEE TRANSACTIONS ON NEURAL NETWORKS, VOL. 14, NO. 5, SEPTEMBER 2003 "VLSI Implementations of Threshold Logic—A Comprehensive Survey"

[17] Hazard-free edge-triggered D flipflop based on threshold gates,J.M.Quintana ,M.J. Avedillo and A Rueda

[18] 'Design of Combinational and Sequential Circuits using Threshold Logic'Mili Sarkar,Subhadeep Nag